Potential for added value in temperature simulated by high-resolution nested RCMs in present climate and in the climate change signal

**Alejandro Di Luca · Ramón de Elía ·
René Laprise**

Abstract Regional Climate Models (RCMs) have been developed in the last two decades in order to produce high-resolution climate information by downscaling Atmosphere-Ocean General Circulation Models (AOGCMs) simulations or analyses of observed data. A crucial evaluation of RCMs worth is given by the assessment of the value added compared to the driving data. This evaluation is usually very complex due to the manifold circumstances that can preclude a fair assessment. In order to circumvent these issues, here we limit ourselves to estimating the *potential* of RCMs to add value over coarse-resolution data. We do this by quantifying the importance of fine-scale RCM-resolved features in the near-surface temperature, but disregarding their skill. The Reynolds decomposition technique is used to separate the variance of the time-varying RCM-simulated temperature field according to the contribution of large and small spatial scales and of stationary and transient processes. The temperature variance is then approximated by the contribution of four terms, two of them associated with coarse-scales (e.g., corresponding to the scales that can be simulated by AOGCMs) and two of them describing the *original* contribution of RCM simulations. Results show that the potential added value (PAV) emerges almost exclusively in regions characterised by important surface forcings either due to the presence of fine-scale topography or land-water contrasts. Moreover, some of the processes leading to small-scale variability appear to be related with relatively simple mechanisms such as the distinct physical properties of the Earth surface and the general variation of temperature with altitude in the Earth atmosphere. Finally, the article includes some results of the application of the PAV framework to the future temperature change signal due to anthropogenic greenhouse gasses. Here, contrary to previous studies centred on precipitation, findings suggest for surface temperature a relatively low potential of RCMs to add value over coarser resolution models, with the greatest potential located in coastline regions due to the differential warming occurring in land and water surfaces.

Keywords Regional climate model · Temperature · Surface forcings · Potential added value · Variance decomposition

1 Introduction

Regional climate modelling consists of using time-dependent large-scale atmospheric fields and ocean surface boundary conditions to drive a high-resolution atmospheric model integrated over a limited-area domain (Giorgi et al. 2001). The models used for this purpose, usually called nested Regional Climate Models (RCMs), have been developed in order to simulate fine-scale climate processes and variability that cannot be resolved by lower resolution Atmosphere-Ocean General Circulation Models (AOGCMs) (Dickinson et al. 1989; Giorgi and Bates 1989). A major motivation in their development was, and

A. Di Luca (✉) · R. Laprise
Centre ESCER (Étude et Simulation du Climat à l Échelle Régionale), Département des Sciences de la Terre et de l'Atmosphère, Université du Québec à Montréal (UQAM), PK - 6530 B.P. 8888, Succ. Centre-ville, Montréal, Québec H3C 3P8, Canada
e-mail: alejandrodiluca@gmail.com

R. de Elía
Centre ESCER (Étude et Simulation du Climat à l Échelle Régionale), Consortium Ouranos, 550 Sherbrooke West, 19th floor, West Tower, Montreal, QC H3A 1B9, Canada

still is, the need of detailed climate information at regional, and even local scales, in order to assess the possible impacts of climate changes in the next decades.

Most state-of-the-art RCMs include a land surface model representing mass, momentum and energy exchanges between the land surface and the atmosphere. Some of them are also coupled with other components of the climate system such as lakes, vegetation and ocean. Atmospheric variables (winds, temperature, pressure and water vapour) at the lateral boundaries and sea surface temperatures (SSTs) and sea ice (SI) concentrations at the surface boundaries are either derived from coarse-resolution AOGCMs or the analyses of observations (reanalyses). Actual horizontal grid spacing used to run multi-decadal RCM simulations varies between 10 and 50 km (e.g., Giorgi et al. 2009) thus implying a jump in resolution of 2–10 compared to AOGCMs. For a detailed discussion about technical issues related with the nesting RCM technique and its potential merits and limitations, readers may refer to one of the several review articles than have been published (Giorgi and Mearns 1991; Wang et al. 2004; Laprise et al. 2008; Rummukainen 2010).

A crucial element in the development of any numerical model trying to describe some aspect of the natural world is its evaluation. That is, in order to quantify how reliable a numerical model is and how confident we can be about its simulations and forecast, model results should be compared with observations in the real world (Randall et al. 2007). For instance, the evaluation of AOGCMs generally proceed by testing their ability to simulate the climate statistics of the recent past. A similar approach can, in principle, be used to test the behaviour of RCMs assuming that high-resolution reliable observations are available (see Prömmel et al. (2010) and references therein).

However, because RCMs are not self-contained tools for climate simulation (i.e., they need boundary conditions from other models or historical analyses), their evaluation must also consider a comparison against the driving data. That is, as pointed out by Prömmel et al. (2010), the key question in RCMs evaluation is not simply whether the RCM-simulated climate compares well with the observed climate, but whether the RCM-simulated climate constitutes a *better* approximation of the observed climate, at least for some particular aspect, than the driving data, i.e., if the RCM produces some added value (AV) over the driving data.

Various articles have been published about the AV issue in the last years (see, for example, Prömmel et al. (2010), Di Luca et al. (2012), Feser et al. (2011) and references therein). Several conclusions can be drawn from the existing literature about AV. First, that RCMs do not seem to add value to the driving data in a consistent and systematic way, but rather suggest that the generation of AV is conditional to a number of factors such as the variable and the climatic statistics of interest, the specific performance of an RCM and the driving data used in the comparison, the characteristics of the region, etc.

An example that illustrates this assertion can be taken from the study of Prömmel et al. (2010). They evaluated the added value in the 2-m temperature field as simulated by the REMO RCM compared to the driving European Centre for Medium-Range Weather Forecasts 40-years reanalysis (ERA40) by using a dense station dataset over the Greater Alpine Region (GAR, 0°–20°E and 40°–50°N). Temporal correlations between observed and ERA40 monthly-mean time series are generally slightly higher than between observations and REMO in most of the GAR with only the exception of the more complex topography sub-regions where REMO shows higher correlations. When looking at 2-m temperature root mean square error, results showed that REMO tends to slightly outperform ERA40 in regions of complex topography but showing little improvement or even degradation of results in flatter sub-regions surrounding the Alps, particularly during the warm season. Hence, the question is still open regarding in which particular cases (i.e., where, when, for which metric, etc.) an RCM will produce an improvement in the representation of the climate compared to the driving data.

A second point is that most of the articles concentrate on an individual pair of RCM results and driving data, thus precluding the generalisation of results. Particularly, AV results derived from a single pair of RCM-GCM could be strongly dependent on the climate models themselves, reflecting differences due to the models' performance instead of general conclusions about the advantages/disadvantages of the RCM technique.

As noted by Feser et al. (2011), most AV studies are based on the comparison between RCMs output and their driving data. The AV arising from this kind of analysis can be considered as a minimum requirement to justify the additional computational effort of RCMs simulations. As pointed out by Laprise et al. (2002), a more complete evaluation of RCMs should be done also in terms of their improvements compared to other statistical and/or empirical downscaling method, generally more affordable and cheaper in terms of computational resources.

With the aim of contributing to the discussion about AV issues, Di Luca et al. (2012) developed a framework nicknamed potential added value (PAV) based on the assumption that RCMs can add value in small scales if and only if they add variance at these fine scales. This methodology is well suited at clarifying the sources of added value in small scales, although the switch from AV to PAV is not without drawbacks. In Di Luca et al. (2012), this framework was used to evaluate the potential of RCMs to add value in a variety of precipitation climate statistics using an ensemble of RCM simulations.

The objective of the present article is threefold: first, to describe a modified version of the PAV framework and a new set of statistics particularly useful for the study of the PAV in near-surface temperature; second, to apply this methodology in order to point out which seasons and regions of North America could benefit from dynamical downscaling of present climate; third, to briefly discuss the difference between added value in present climate and in the climate-change signal. We are aware that, while near-surface temperature is a key variable because it is widely used in climate studies and in climate change projections, it is not necessarily the best variable to assess the benefits of using high-resolution climate models. Indication about the PAV associated with temperature statistics, however, can be of great interest to those using it in climate and climate change studies.

The paper is structured as follows. The next section presents a brief description of the data used. Section 3 describes the general framework used to evaluate the PAV together with the variance decomposition used to separate large- and fine-scale contributions. Section 4 presents temperature results separated in three parts: the potential added value in present climate simulations, some discussion of the complexity of this AV, and the PAV in the temperature climate-change signal for future projections. Lastly, concluding remarks are given in Sect. 5.

2 Data

The RCM simulations used in this study were provided by the North American Regional Climate Change Assessment Program (NARCCAP; http://www.narccap.ucar.edu/; Mearns et al. 2009). In NARCCAP, six RCMs were run with a horizontal grid spacing of about 50 km over similar North American domains covering Canada, United States and most of Mexico. Acronyms, full names and a reference, and the modelling group of each RCM are presented, respectively, in the first three columns in Table 1.

The NARCCAP experiments include simulations of contemporary climate using lateral boundary conditions (LBCs) derived from the National Centers for Environmental Prediction (NCEP) Department of Energy (DOE) global reanalysis (Kanamitsu et al. 2002) for the 25-year period between 1980 and 2004. NARCCAP also comprises RCM simulations driven at the lateral and lower boundary conditions by AOGCM simulations for present (1971–2000) and future climate (2041–2070) using the A2 scenario (Mearns et al. 2009). Four AOGCMs are used to drive the RCMs: the Canadian Global Climate Model version 3 (CGCM3, Flato 2005), the NCAR Community Climate Model version 3 (CCSM3, Collins et al. 2006), the Geophysical Fluid Dynamics Laboratory Climate Model

version 2.1 (GFDL, GFDL Global Atmospheric Model Development Team 2004) and the United Kingdom Hadley Centre Coupled Climate Model version 3 (HadCM3, Gordon et al. 2000). The fourth column in Table 1 provides the LBCs used to drive each RCM. A total of six RCM-AOGCM pairs are used here to analyze the climate change signal, with two RCMs (CRCM and RCM3) driven by two AOGCMs and two RCMs (WRFG and HRM3) driven by only one AOGCM. Simulations using the ECP2 RCM driven by AOGCMs were not available at the time this research was carried out. Similarly, due to technical problems we could not process the output from the MM5I-CCSM simulation and so these results are not included in the analysis.

For each RCM simulation, several 3-hourly variables are available in their original map projection; but in this article we will concentrate only on 2-m temperature. Reanalysis driven RCM simulations use AMIP II sea surface temperature (SST) and sea ice (SI) concentration observations as lower boundary conditions (Kanamitsu et al. 2002). AOGCM driven RCM simulations use SST and SI from the AOCGM data. In both reanalysis- and AOGCM-driven simulations, SST and SI surface boundary conditions are updated every 6 hours by using a linear interpolation between consecutive monthly-mean values. Similarly, boundary conditions are interpolated from the low resolution to the ~50-km grid meshes by using a linear interpolation in the horizontal.

3 Methodology

3.1 Potential added value framework

The general conceptual framework used to study the PAV in the temperature field simulated by an ensemble of RCMs is described in Di Luca et al. (2012); but in the present work some important methodological modifications are introduced. In that article, two types of AV were defined according to the spatial scales in which the AV would be produced. Small-scales AV (AV^{ss}) refers to those RCM improvements occurring in scales that are not explicitly resolved by the driving data. Large-scales AV (AV^{ls}) denotes improvements in those scales that are common to both RCMs and the lower resolution driving data.

Given that the main objective of RCMs is to add fine-scale features to the coarser AOGCMs, there is a general consensus in the RCM community (e.g., Feser 2006; Prömmel et al. 2010) that the primary added value of RCMs is related with AV^{ss}. Much less agreement exists about whether or not RCMs can generate AV at large scales. Although some authors [e.g., Mesinger et al. (2002) and Veljovic et al. (2010)] sustain a potential improvement

Table 1 Acronyms, full names (reference) and modelling group of RCMs involved in the NARCCAP project. Column 4 indicates the LBCs used to drive each RCM

RCM	Full name (Reference)	Modelling group	LBCs
CRCM	Canadian Regional Climate Model (version 4.2.0) (Caya and Laprise 1999)	Ouranos / UQAM	NCEP-DOE CGCM3 CCSM
ECP2	Experimental Climate Prediction Center Regional Spectral Model (Juang et al. 1997)	UC San Diego Scripps	NCEP-DOE
HRM3	Hadley Regional Model (version 3) (Jones et al. 2004)	Hadley Centre	NCEP-DOE HadCM3
MM5I	MM5 - PSU/NCAR mesoscale model (Grell and Stauffer 1993)	Iowa State University	NCEP-DOE
RCM3	Regional climate model (version 3) (Giorgi et al. 1993)	University of of California at Santa Cruz	NCEP-DOE GFDL CGCM3
WRFG	Weather research and forecasting model (Leung et al. 2005)	Pacific Northwest National Laboratory	NCEP-DOE CCSM

of large-scale features through the use of RCMs, a large part of the RCM community (e.g., Castro et al. (2005) and Laprise et al. (2008)) seems to promote the use of large-scale nudging thus reducing large-scale differences between the RCM and the driving data.

As in Di Luca et al. (2012), the experimental design used here to study the PAV is explicitly conceived to investigate AV^{ss}, that is, whether RCMs can add value in small scales. Since no attempt will be made here to identify AV^{ls}, the failure of a given RCM to potentially generate AV^{ss} should not be taken to imply that the RCM is incapable of producing some AV through AV^{ls}.

The PAV framework is based on the idea that a prerequisite condition for an RCM to produce AV^{ss} is that the RCM must be able to generate non-negligible variability in spatial scales finer than the smallest scale represented by the lower resolution driving data (i.e., fine scales). The contribution of fine-scale processes in the description of given climate statistics can then be used to quantify the PAV of a given RCM simulation. The term *potential* in this definition accounts for the fact that the presence of small scales is not a sufficient condition to have AV^{ss} because RCM-simulated fine scales may not necessarily resemble the observed ones.

Instead of directly comparing RCM simulations and driving data statistics, a perfect-model approach is used here to determine the relative importance of fine-scale features. It is assumed that the statistics of the driving data can be approximated by aggregating the high-resolution (e.g., ∼50-km grid spacing) field simulated by an RCM into a coarse grid mesh with an horizontal spacing similar to that used by the driving reanalysis or model. That is, we consider that a high-resolution field upscaled into a 300-km grid (i.e., a jump in resolution of around six in the linear

horizontal dimension compared to RCMs) generates what we call a virtual GCM (VGCM) field whose statistics behave as those from a real GCM (i.e., as a model with 300-km grid spacing). For a detailed discussion of the consequences of using this approximation the reader is referred to Di Luca et al. (2012).

Differences between an RCM and its corresponding VGCM can be expressed using the Reynolds decomposition technique (Stull 1988). Let us consider an RCM-simulated time-varying field $T_{i,k}$, with index i identifying the spatial dimension and k the temporal dimension, within 300-km side regions containing about 36 RCM grid points. By applying Reynolds decomposition we can separate the quantity $T_{i,k}$ in its spatial average and fluctuations around this average as follows,

$$T_{i,k} = \langle T_k \rangle + \widehat{T}_{i,k}, \tag{1}$$

where $\langle T_k \rangle$ is the 300-km spatial average temperature, at each time step, representing a low-resolution version of the RCM (i.e., the virtual GCM time series), and $\widehat{T}_{i,k}$ represents the time series departures of the 50-km grid spacing field from the 300-km average field. Figure 1a shows the location of MM5I RCM grid points in its original grid mesh (blue light squares) and the resulting VGCM grid point (black cross) in an individual region centred on −118.3° of longitude and 32.8° of latitude.

In a similar way as done with the spatial dimension of the $T_{i,k}$ field, Reynolds decomposition can be applied over the temporal dimension of both terms in Eq. (1) to obtain,

$$T_{i,k} = \overline{\langle T \rangle} + \langle T_k \rangle' + \overline{\widehat{T}_i} + \widehat{T}'_{i,k}, \tag{2}$$

with $\overline{\langle T \rangle}$ the spatio-temporal mean, $\langle T_k \rangle'$ the temporal fluctuation of the spatial mean, $\overline{\widehat{T}_i}$ the temporal mean of

Fig. 1 a Individual 300-km side region centred on $-118.3°$ of longitude and $32.8°$ of latitude and **b** the 288 regions use in the analysis. The total domain of analysis is common to all 6 RCM domains and each sub region has the same dimensions (i.e., 300 km by 300 km)
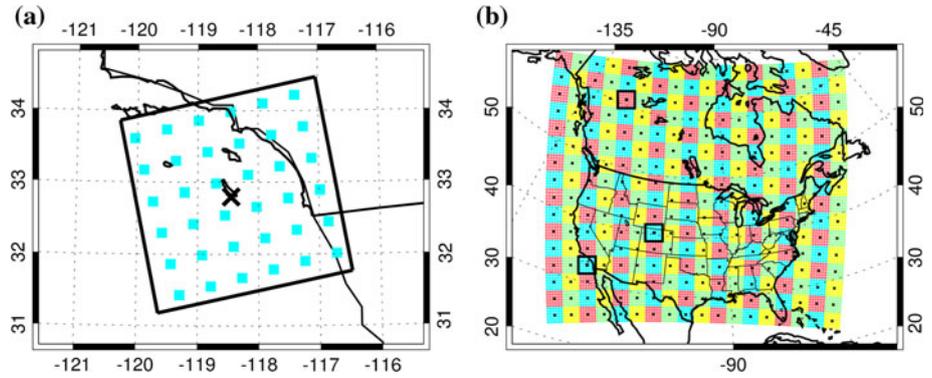
spatial deviations and $\widehat{T}'_{i,k}$ the spatio-temporal fluctuations of temperature. The Reynolds decomposition is performed in each individual VGCM grid box and so the spatial average is computed over 300-km side regions. Time-averaged values are computed using 20 (19) summer (winter) 3-hourly time series between 1981 and 2000. Winter season is defined as the three months between December and February and summer season is defined by the months between June and August.

3.2 Variance decomposition analysis and PAV quantities

By using properties of the variance operator and assuming that the temporal fluctuations of the spatial mean are independent of the spatio-temporal fluctutations (see Appendix A for more details), the variance of Eq. (2) can be expressed as,

$$\begin{aligned}
\sigma^2 = Var(T_{i,k}) &= Var(\langle T_k \rangle' + \overline{\widehat{T}_i} + \widehat{T}_{i,k}') \\
&\approx Var(\langle T_k \rangle') + Var(\overline{\widehat{T}_i}) + Var(\widehat{T}_{i,k}') \quad (3) \\
&\approx \sigma^2_{tVGCM_k} + \sigma^2_{sRCM_i} + \sigma^2_{tRCM_{i,k}},
\end{aligned}$$

with $\sigma^2_{tVGCM_k}$ denoting the temporal variance of the spatial-mean term, $\sigma^2_{sRCM_i}$ the spatial variance of the RCM time-averaged temperature in each VGCM grid box and $\sigma^2_{tRCM_{i,k}}$ the variance of the residual fluctuations. The approximation in Eq. (3) results from the assumption that the covariance term between $\langle T_k \rangle'$ and $\widehat{T}'_{i,k}$ is much smaller than the other contributions. In practice, when applied to temperature, the covariance term is at least one order of magnitude smaller than the sum of the RCM variance contributions.

The term $\sigma^2_{tVGCM_k}$ is assumed to represent what a low-resolution GCM can produce. The others two terms are the stationary ($\sigma^2_{sRCM_i}$) and transient ($\sigma^2_{tRCM_{i,k}}$) components of the RCM original contributions to the total variance. They represent the PAV of the RCM over the virtual GCM:

$$PAV = \sigma^2_{sRCM_i} + \sigma^2_{tRCM_{i,k}}. \quad (4)$$

A negligible value of the PAV quantity would suggest that the total variance is not affected by the high-resolution information but completely determined by its low resolution part. A normalized form of Eq. (4) can be defined in order to quantify the relative influence of RCM components in the total variance:

$$rPAV = \frac{\sigma^2_{sRCM_i} + \sigma^2_{tRCM_{i,k}}}{\sigma^2}, \quad (5)$$

with $rPAV$ varying between 0 and 1, thus allowing for a more proper comparison of PAV results across different regions and seasons. Again, $rPAV \sim 0$ would suggest that no RCM information is needed to determine the total variance in that region, while $rPAV \sim 1$ would mean that all the variance comes solely from the fine-scale information simulated by the RCM with no influence from the VGCM term.

In order to evaluate the regional dependence of PAV quantities, the variance analysis is performed over 300-km side, non-overlaped, regions that are common to all RCM domains (see Fig. 1b). The VGCM grid mesh contains a total of 288 such grid boxes. The number of RCM grid points inside any given VGCM grid box depends on the specific map projection and the horizontal grid spacing of each RCM. For example, WRFG and MM5I have 36 grid points in every region at all latitudes because they use a 50-km Lambert conformal projection that conserves the distance between two consecutive grid points. ECP2 and CRCM models' regions contain a varying number of grid points with a minimum of 25 and a maximum of 66 in the northern and southern parts of the domain respectively.

In this paper results are showed only for the variance decomposition of the 3-hourly RCM time series, but the analysis was conducted also for daily and 16-day time series.

4 Results

4.1 PAV in current climate

Figure 2 shows the RCM ensemble-mean total variance of the temperature field in cold season together with the three terms derived using Reynolds decomposition as explained in Sect. 3.2. Ensemble-mean variance terms are obtained by simply computing the arithmetic average over each variance term in Eq. (3) as estimated from the individual RCMs. For example, in order to get the ensemble-mean of the $\sigma^2_{tVGCM_k}$ term, we computed $\sigma^2_{tVGCM_k}$ for each RCM simulation and then averaged over the six RCM variance estimations.

The ensemble-mean total variance term (see Fig. 2a) shows values between ~ 2 K^2 (~ 1 K as standard deviation), in some subtropical oceanic regions, and ~ 130 K^2 (~ 11 K) in continental and high-latitude regions with a domain average of 54 K^2. As is clear by comparing Fig. 2a and b, most of the temperature variance is generated by the temporal fluctuation of the spatial-mean term (i.e., the *tVGCM* term). The *tVGCM* term is influenced by a wide range of processes with time scales larger than 3 hours and up to decadal variability. Inspection of variance terms resulting from the variance decomposition analysis shows similar spatial patterns in the 3-hourly, the daily and the 16-days total variance fields. This

suggests that that the general spatial pattern of variability seen in Figs. 2a and 2b is largely induced by intraseasonal and interannual variability, that is those wavelengths not filtered out by 16-day average or less. Particularly in the south part of the domain, there is an important influence of sub-daily scale variability evidenced by a reduction of variance values from the 3-hourly total variance field to the daily one. Also, particularly in the north part, synoptic variability seems to play an important role by showing an increase on the total variance between the daily and the 16-days analysis.

It is also clear in Fig. 2a that 2-m temperature shows weak temporal variability over oceanic regions with values generally smaller than 10 K^2 due to the relatively weak temporal and spatial variability of SSTs, compounded by the fact that SSTs are updated only on a monthly basis in NARCCAP RCM simulations.

Figure 3a, b and c show an 8-day period of the *tVGCM_k* time series in January of 1981 for three different regions located in the West Coast (centred on $-118.3°$ of longitude and 32.8° of latitude), the Rocky Mountains (centred on $-106.1°$ of longitude and 40.3° of latitude) and in northern Canada (centred on $-127.3°$ of longitude and 59.9° of latitude). All three regions are designated with black squares in Fig. 1b. Because most grid points in the West Coast region are water grid points, this region shows relatively weak temporal variability, mainly dominated by the

Fig. 2 Ensemble-mean variance decomposition applied to the 3-hourly temperature field in cold season for **a** the total variance, **b** the virtual GCM variance, **c** the RCM stationary variance and **d** the RCM transient variance
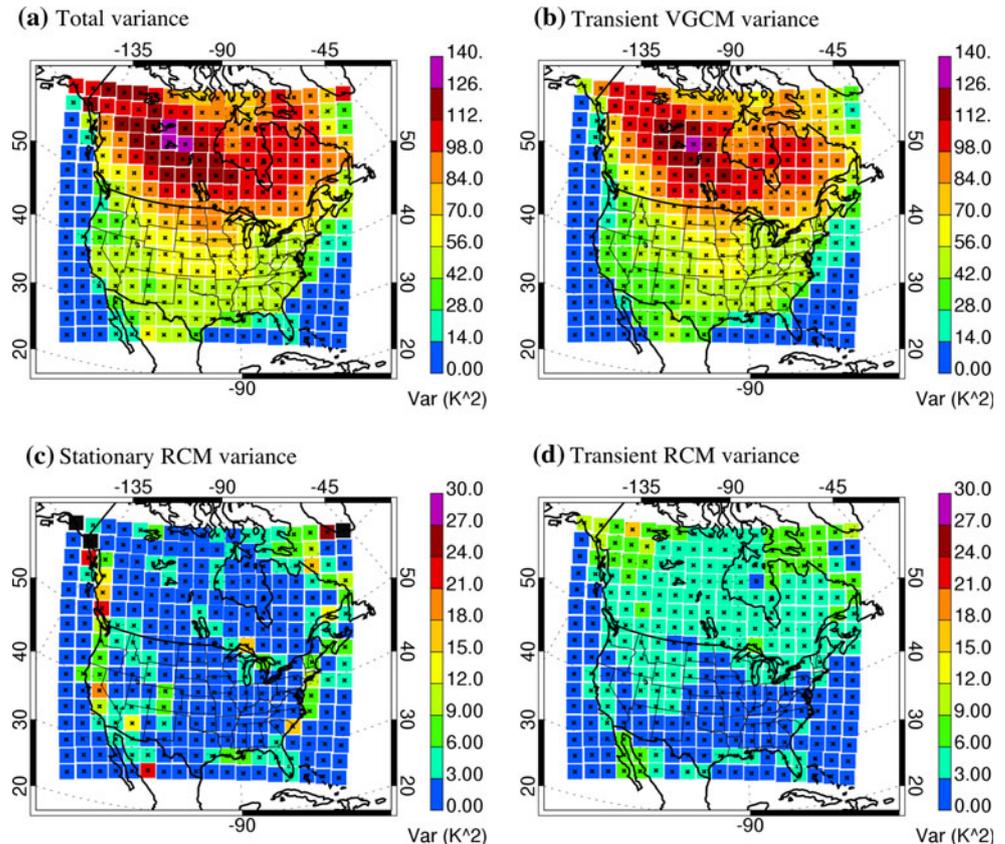
land diurnal cycle. The other two regions show stronger day-to-day variability (they contain only land grid points), mainly related with the passage of synoptic-scale systems.

Figure 2c and d show the ensemble-mean temperature spatial variances of the temporal mean (i.e., $\sigma^2_{sRCM_k}$ stationary term) and the spatio-temporal fluctuation (i.e., $\sigma^2_{tRCM_{i,k}}$ transient term) terms in cold season (note that the colour scale is different from Fig. 2a and b). Both terms are of the same order of magnitude, with domain-average variances of about 4 K^2, but spatial patterns show significant differences.

The ensemble-mean spatial variance of the RCM stationary term tends to maximize in regions where the topographic and/or the land-water contrast forcings are important. The topographic forcing creates stationary temperature differences across grid points mainly due to

the general variation of mean temperature with altitude. A more detailed example of the topographic source of stationary variance is given in Fig. 3e (see central United States black square in Fig. 1b). This figure shows the cold-season 20-year time-averaged temperature in MM5I grid points inside the Rocky Mountains' region characterised by significant fine-scale topography. The altitude effect induces mean horizontal temperature gradients of the order of 10 K / 250 km that result in relative large $\sigma^2_{sRCM_i}$ values of the order of 8 K^2.

Land-sea contrast also induces stationary temperature gradients simply because the time-averaged temperature in sea/lakes can be different from the mean temperature over land surfaces. Figure 3d shows the cold-season temporal-mean temperature in MM5I grid points for the region located in the West Coast (see southernmost black square
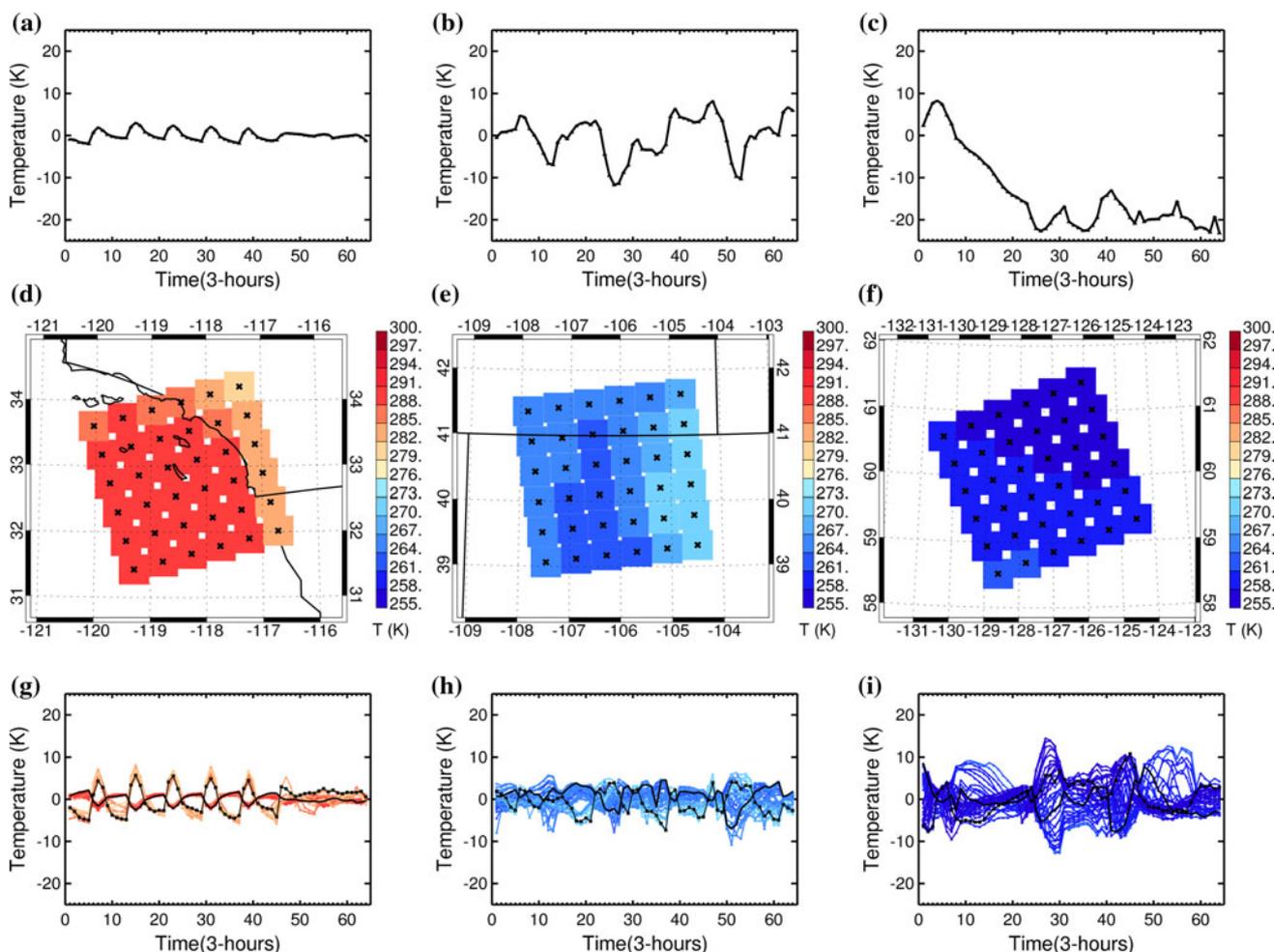
Fig. 3 8-day period spatial-mean time series (VGCM term; top panels), 20-years time-averaged 2-m temperature (sRCM term; middle panels) and 8-day period fine-scale transient term (tRCM term; bottom panels) in cold season. Left panels correspond to a region located in the West Coast of United States; centre panels correspond to a region with important topographic forcing, and right panels correspond to a flat region in northern Canada. Results correspond to the MM5I RCM and the several lines in bottom panels represent the 2-m temperature evolution in individual grid points with colours given by the colorbar scale in middle panels. All three regions are shown in Fig. 1b

in Fig. 1b). Relatively large values of $\sigma^2_{sRCM_i}$ appear in this region due to the differences between the warm temperatures in MM5I grid points located over the Pacific Ocean and those grid points in the colder land. This effect is even more pronounced in some regions located along the East Coast due to the stronger land-sea contrast induced by the warmer SSTs over the Gulf Stream (see Fig. 2c).

Figure 4 shows the fine-scale stationary variance term for each RCM in cold season. The more important intermodel differences appear over the Great Lakes, the Hudson Bay and the Labrador Sea. The absence of continental contrast in the RCM3 stationary term (see Fig. 4e) simply results from its land-sea mask that does not contain any lake. In some regions (e.g., Great Lakes), differences across RCMs appear to be related with differences in the land-water fraction masks used by each RCM (see Appendix B for more details). In other regions (e.g., Labrador Sea), differences across RCMs seem to be related with more fundamental aspects such as the representation of latent and sensible heat fluxes in each RCM.

Over oceanic and relatively flat regions (in the central eastern part of United States and most of Canada), the variance of the fine-scale stationary term is very small, with values smaller than 1 K^2. The MM5I RCM timeaveraged temperature field in the region located in northern Canada (see Fig. 3f) shows that, in flat continental regions, horizontal temperature gradients are weaker than in mountainous or coastal regions with a south-north gradient

of about 5 K / 400 km due to the general increase of temperature to the Equator (note that the scale range is the same in Fig. 3d, e and f). Interestingly, values larger than 1 K^2 appear in some oceanic regions near the East Coast of US and Canada, a feature that arises in the ensemble-mean variance (see Fig. 2c) and in individual RCM simulations (see Fig. 4). This signature is related with the strong stationary SST gradients across the Gulf Stream in these latitudes since all RCMs share the same SSTs, with changes in the time-averaged temperature of about 10 K / 300 km in some of these regions.

The ensemble-mean variance of the RCM transient term is shown in Fig. 2d and individual RCM transient terms are shown in Fig. 5. In general, several mechanisms can produce transient PAV. By its definition, there will be some transient PAV if there exists 50-km spatial differences in the temporal variability of the 2-m temperature. The comparison of the transient term variance derived using 3-hourly and daily time series shows that, particularly in the southern part of the domain, most transient variability comes from temporal scales shorter than 24 h. The process that seems to dominate sub diurnal variability arises from the different diurnal cycle across RCM grid points in a given region. This effect tends to be larger in coastal regions where land grid points have a much more intense diurnal cycle than water grid points explaining the relative maxima of transient PAV in the West Coast (e.g., Baja California coast), the south US coast and Great Lakes regions.
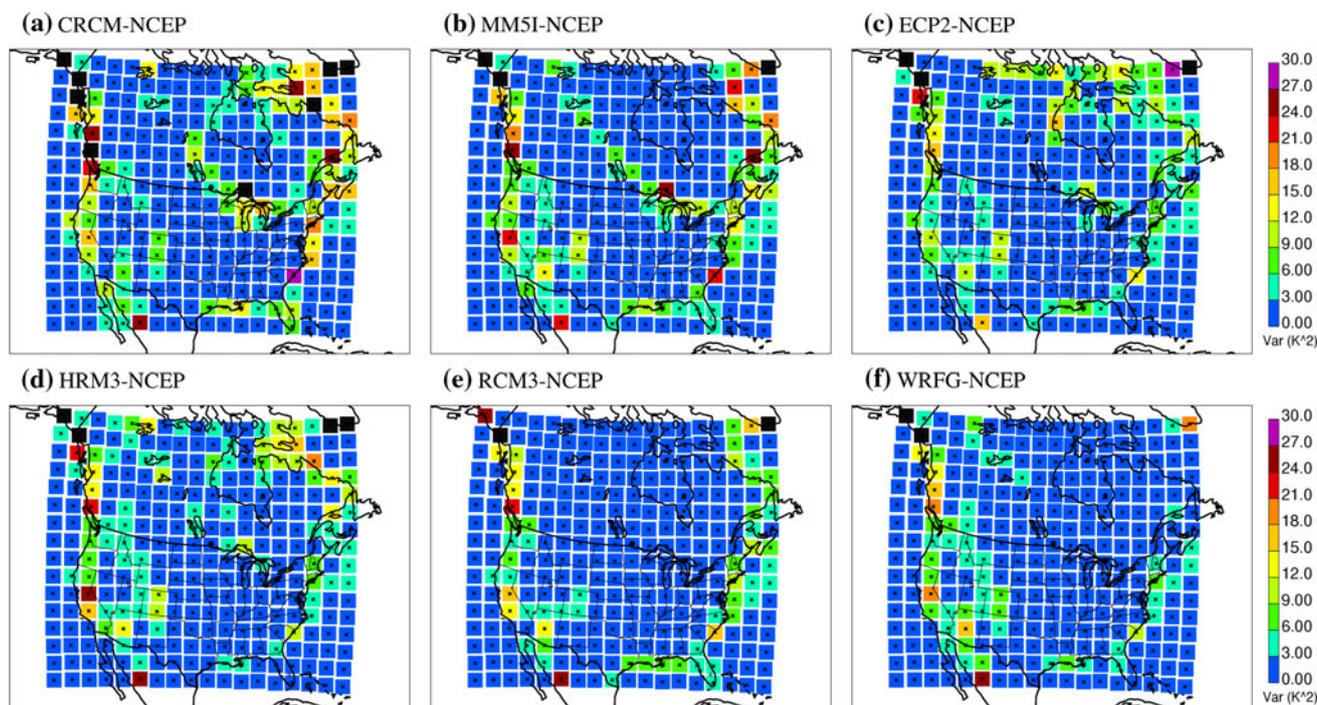
Fig. 4 RCM stationary variance term computed from individual RCM simulations in cold season
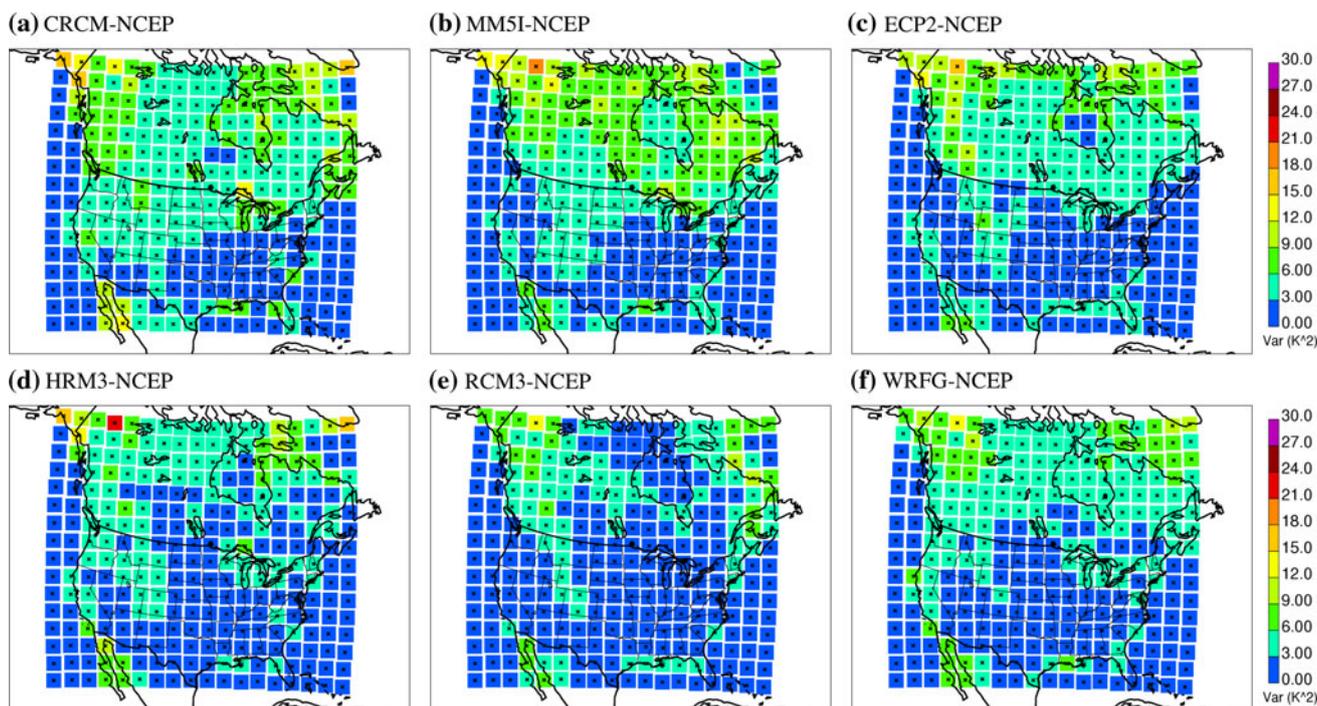
Fig. 5 RCM transient variance term computed from individual RCM simulations in cold season

In order to better understand the diurnal cycle spatial variability and the sub-daily transient term, Fig. 3g–i show the transient term $tRCM_{i,k}$ for an 8-day period (similar as that used in Fig. 3a–c) in the same three regions as before. In the West Coast region (Fig. 3g), it is clear that the transient variability (at least in the first 6 days) is dominated by the different diurnal cycle in oceanic and land grid points. Differences between land (ocean) grid points and the spatial-mean term ($tVGCM_k$) appear as a positive (negative) anomaly during day-time and as a negative (positive) anomaly during night-time respectively. The diurnal cycle is, as expected, stronger over land than over ocean grid points.

Figure 3h shows that the topographic forcing induces little sub diurnal transient variability because, even if time-averaged temperatures are different across grid points, their diurnal cycle is very similar. In the northern Canada region (see Fig. 3i), the influence of the diurnal cycle is very small due to the weak solar forcing in high latitudes in this time of the year.

In cold season, the ensemble-mean fine-scale transient term (see Fig. 2d) systematically shows higher values in continental compared to oceanic regions. This continental transient component of PAV is a robust feature that appears in any single model experiment as shown in Fig. 5. The inspection of the fine-scale transient term computed using daily and 16-day time series (not shown) reveals that differences between oceanic and continental regions are present when looking at daily time series but do not appear when considering 16-days transient variability term, which seems to imply that the continental-oceanic feature is probably related to synoptic variability.

A process that can be important to explain continental-oceanic differences relates to middle-latitude synoptic systems and their associated surface fronts. The passage of a synoptic-scale perturbation over a given region (generally from west to east in middle latitudes) induces a spatial gradient of temperature that varies in time (as the system moves) and in space (relative position compared to the front). The spatial gradient induced by the perturbation is larger over continental compared to oceanic regions simply because of the important damping from the ocean.

The passage of synoptic-scale systems is also probably related to the general increase of the transient term to the northern part of the domain in cold season. This north-south gradient of the transient term is seen in the ensemble-mean term (see Fig. 2d) and in most of individual RCM terms, particularly in the north- western and eastern parts of the domain (see Fig. 5). Figure 3h and i illustrate the influence of synoptic variability in the transient term over continental regions. The range of transient variability is of the order of ~ 10 K in the Rocky Mountains region and of the order of ~ 20 K in the northern Canada region.

Figure 6 shows the RCM ensemble-mean total variance and its decomposition terms as in Fig. 2 for the warm season. In this season, the ensemble-mean total variance (standard deviation) shows values varying from ~ 1 K^2 in subtropical oceanic regions, to ~ 75 K^2 (~ 9 K) in

Fig. 6 As in Fig. 2 but for warm season computations
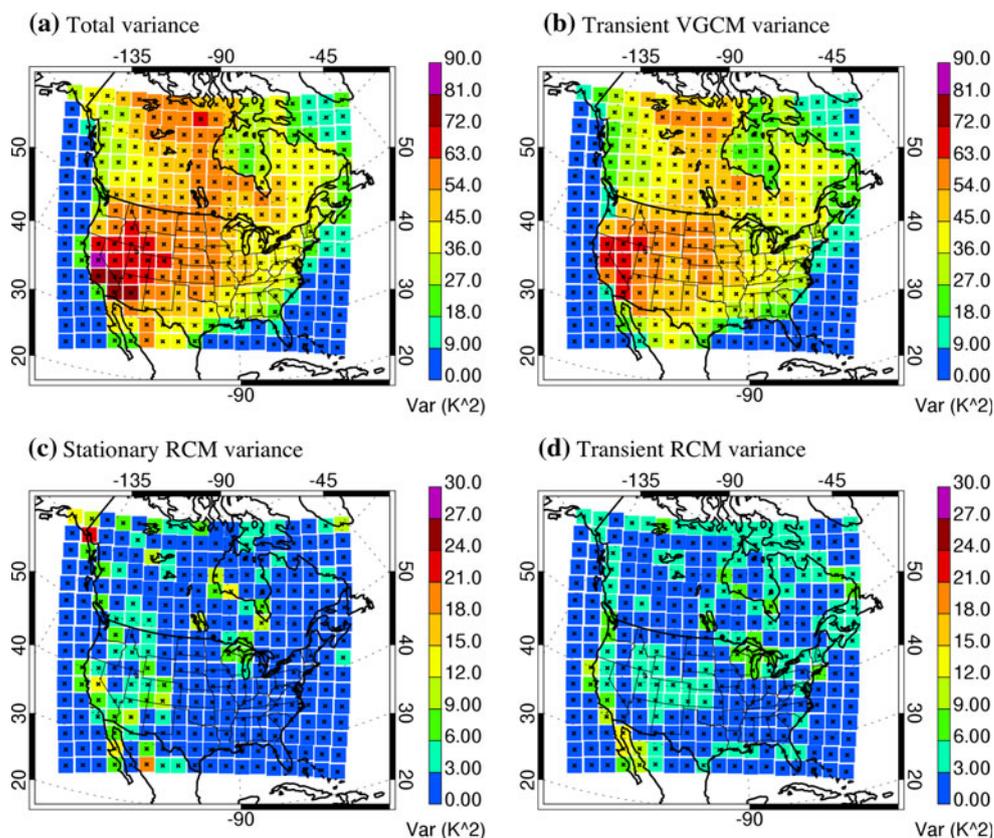
continental mid-latitude regions, with a domain-average value of 29 K^2. Again, most of the total variance is contained in the temporal fluctuation of the spatial-mean term. In this case, the virtual-GCM term shows maximum values in the central eastern part of the conterminous United States, at approximately 40° of latitude, as a result of a combination of intraseasonal and interannual variability, synoptic variability and the very large diurnal cycle in this region as a product of the large solar forcing and the relatively dry soils. A secondary maximum appears to the west of the Hudson Bay mainly due to interannual and synoptic variability. Figure 7a–c show an 8-day period of the VGCM time series for the same regions as in Fig. 3. Comparing with cold season results, the most outstanding feature is that the diurnal cycle tends to dominate temporal variability everywhere, although modulated by longer time scale processes.

Figure 6c and d show respectively the ensemble-mean stationary and transient variance terms in warm season. As in cold season, the stationary and the transient terms show domain-average values of 2 and 3 K^2 respectively. The most important differences between the ensemble-mean stationary term in warm compared to cold season are the lower values in the North American East Coast and the

higher values over the Hudson Bay coast: these two features appear in every RCM simulation (see Figs. 4 and 8).

As in cold season, the transient term in warm season (see Fig. 9) shows higher values in continental compared to oceanic regions and maximum values occur in some regions where the land-water contrast forcing is important such as the West Coast and the Great Lakes regions. However, particularly on northern regions and in flat regions with little land-sea contrast, the fine-scale transient term is generally smaller than in cold season probably due to the weaker synoptic-scale variability (see Fig. 3h and i).

When looking at the ensemble-mean and individual RCM transient terms, important differences between cold and warm seasons appear in regions with significant influence of lakes. In particular, warm-season transient variances show higher values than cold-season ones probably due to the stronger contrast between water and land in this season compared to the contrast between ice and snow/permafrost in cold season. That is, in cold season, the land-water contrast forcing associated with the presence of lakes is partially hidden due to the presence of snow-ice layers in both land and water. The more important land-sea contrasts together with the much stronger diurnal cycle in warm season tend to increase transient term values.
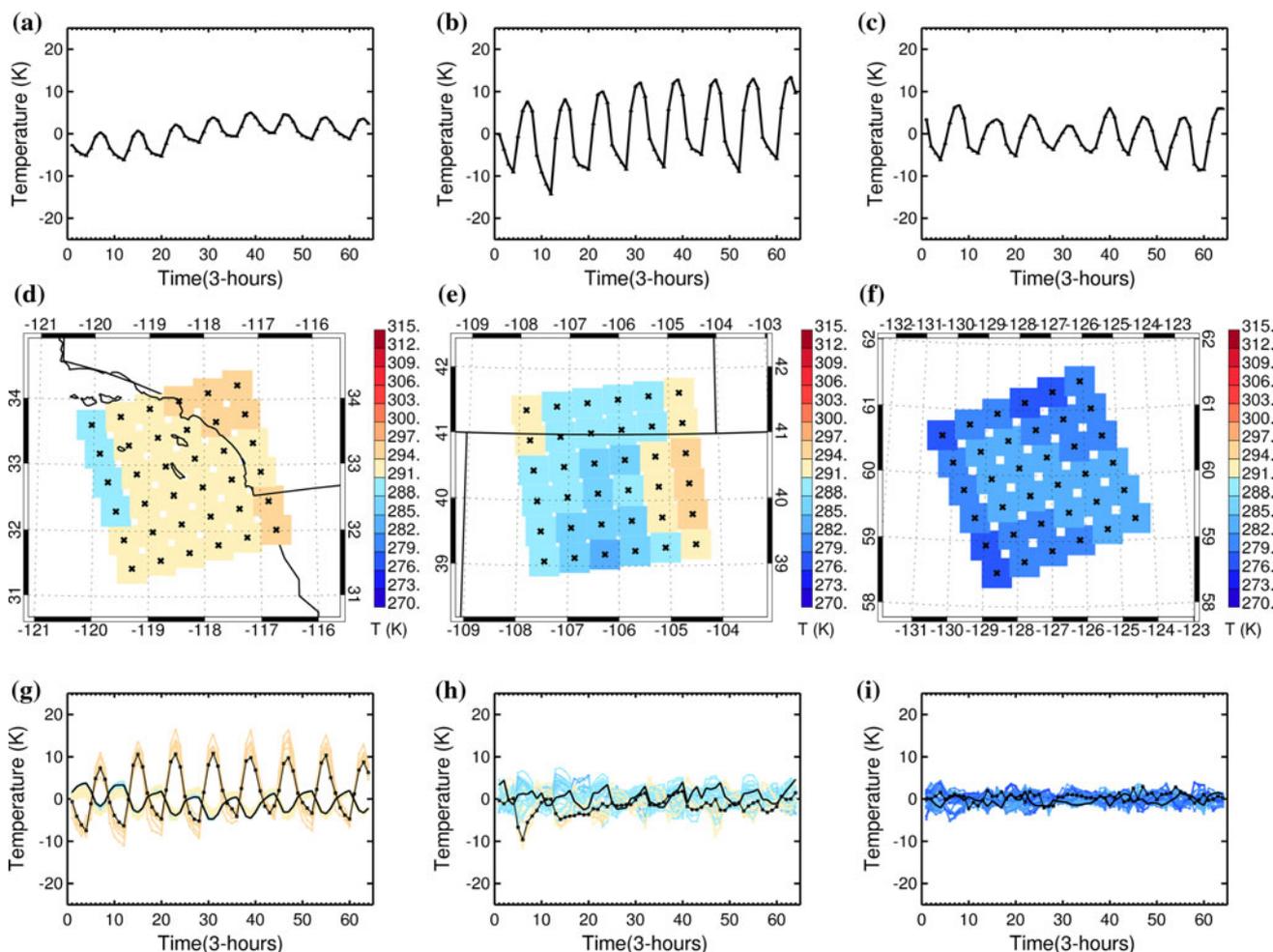
Fig. 7 As in Fig. 3 but for warm season computations

4.2 Stationary and transient components of relative PAV

As defined in Sect. 3, the relative PAV measure [rPAV; see Eq. (5)] is given by the fraction of the total variance that is accounted by the sum of the stationary and the transient RCM terms (i.e., the original, genuine contribution of the RCM field) to the total variance. Figure 10 shows the RCM ensemble-mean *rPAV* in cold (Fig. 10a) and warm (Fig. 10b) seasons. Qualitatively, results are quite different from those derived using the absolute variance terms. For example, some oceanic regions (e.g., south Pacific regions) show higher *rPAV* values than flat continental regions even if PAV terms were higher in the later regions because the total variance in the denominator in Eq. (5) tends to be larger over land than over ocean. Similarly, some mountainous regions with relatively large stationary variance values show very little *rPAV* due to the large total variance in these regions.

In both seasons, ensemble-mean *rPAV* values are generally smaller than 15 % and relative maxima are related with regions strongly influenced by land-sea contrast forcing. The RCM contributions to the total variance are higher in warm compared to cold season with a domain average of 16 and 5 % respectively. At least in part, seasonal differences seem to be related to the general intensification of the diurnal cycle of the land-sea contrast forcing in warm season, particularly in mid-latitude and northern regions (e.g., Great Lake regions).

In cold season, relative maxima are found all along the North American West Coast and the south-east coast of the United States. In warm season, relative maxima are related mostly with coastline regions either near the sea or due to the presence of lakes.

Figure 10c and d show the fraction of *rPAV* that is explained by the stationary and the transient terms computed as $2\sigma^2_{sRCM_i}/(\sigma^2_{sRCM_i} + \sigma^2_{tRCM_{i,k}}) - 1$. Positive (negative) values denote those regions where the stationary (transient) term tends
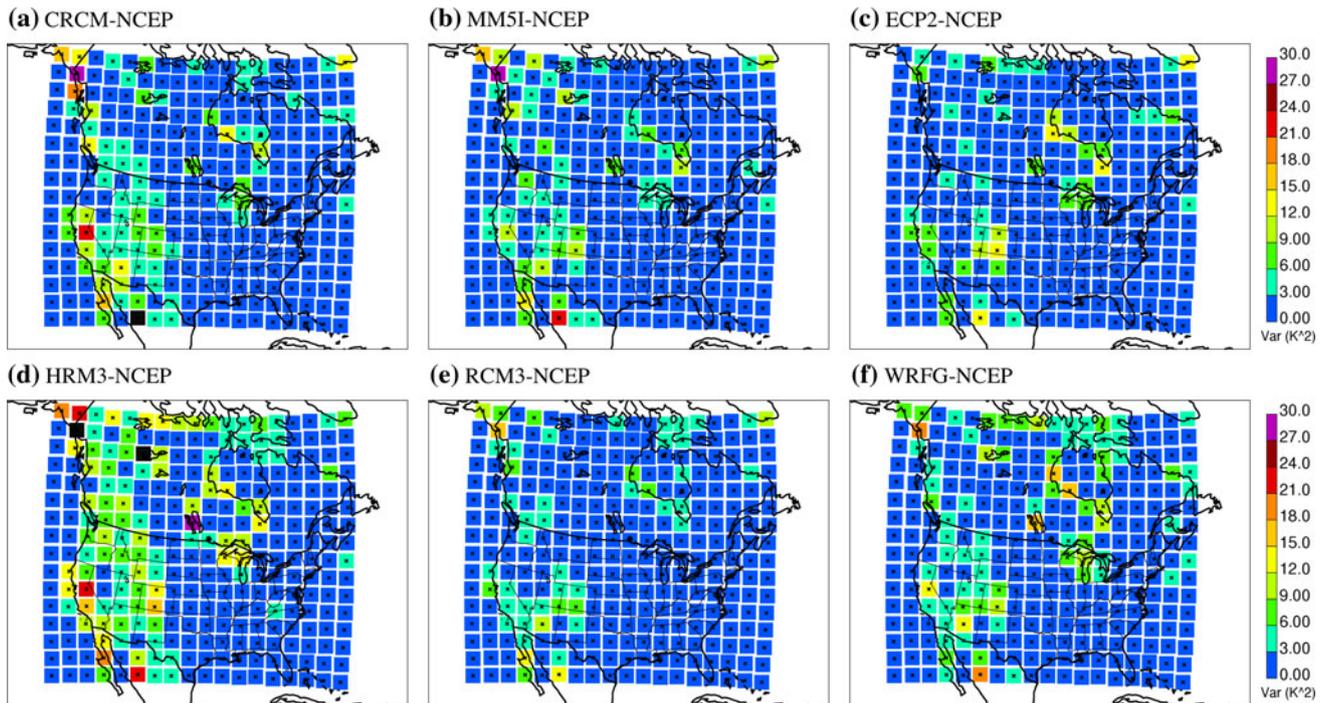
Fig. 8 As in Fig. 4 but for warm season computations
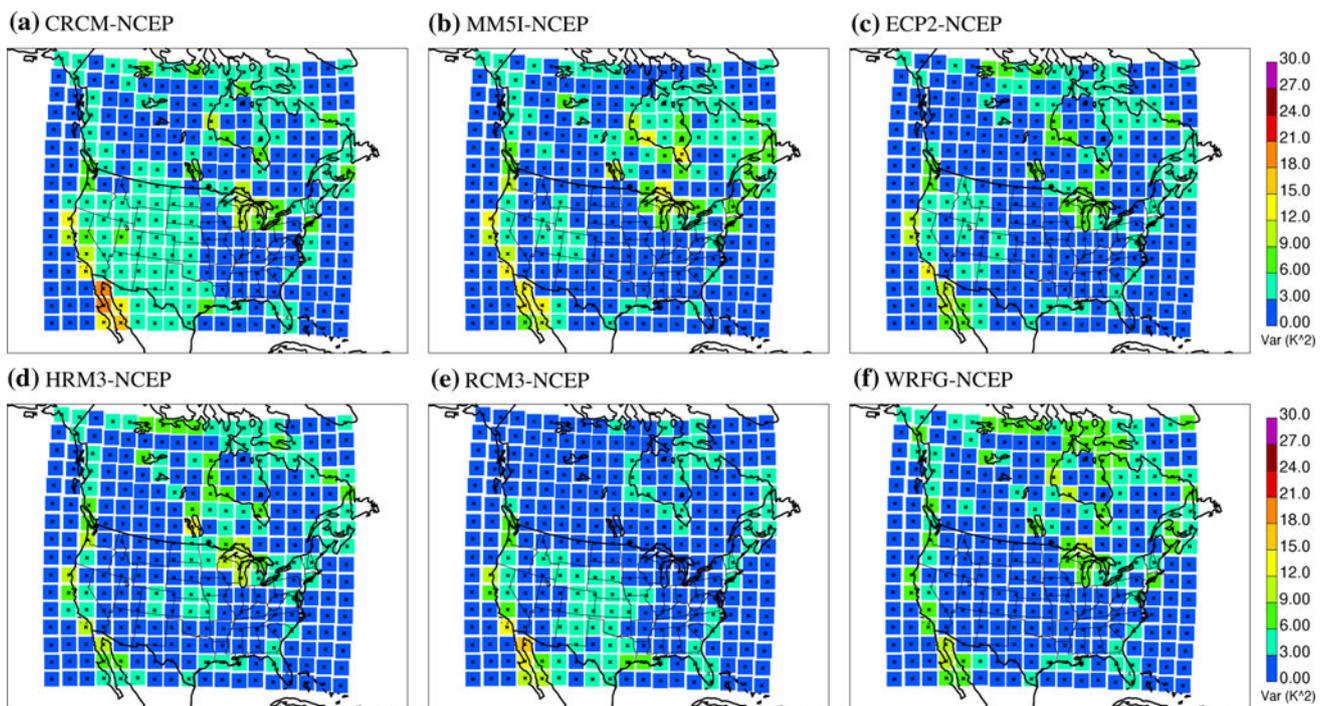
Fig. 9 As in Fig. 5 but for warm season computations

to be dominant with values equal to 1 (−1) denoting that all the *rPAV* comes from the stationary (transient) term. Black asterisks denote those regions where *rPAV* is larger than 15 %.

In both seasons, ensemble-mean *rPAV* values larger than 15 % are only found in regions where surface forcings are

important, either due to complex topography or land-water contrasts. The number of regions with *rPAV* larger than 15 % is larger in warm (131 regions out of 288) than in cold (107 regions) season. Most of these regions appear in the northern part of the domain mainly due to the lower

Fig. 10 Ensemble-mean *rPAV* in (**a**) cold and (**b**) warm seasons and the fraction of *rPAV* coming from the stationary and transient terms in (**c**) cold and (**b**) warm seasons. Black crosses in bottom panels denote those regions where the ensemble-mean *rPAV* signal is larger 10 %
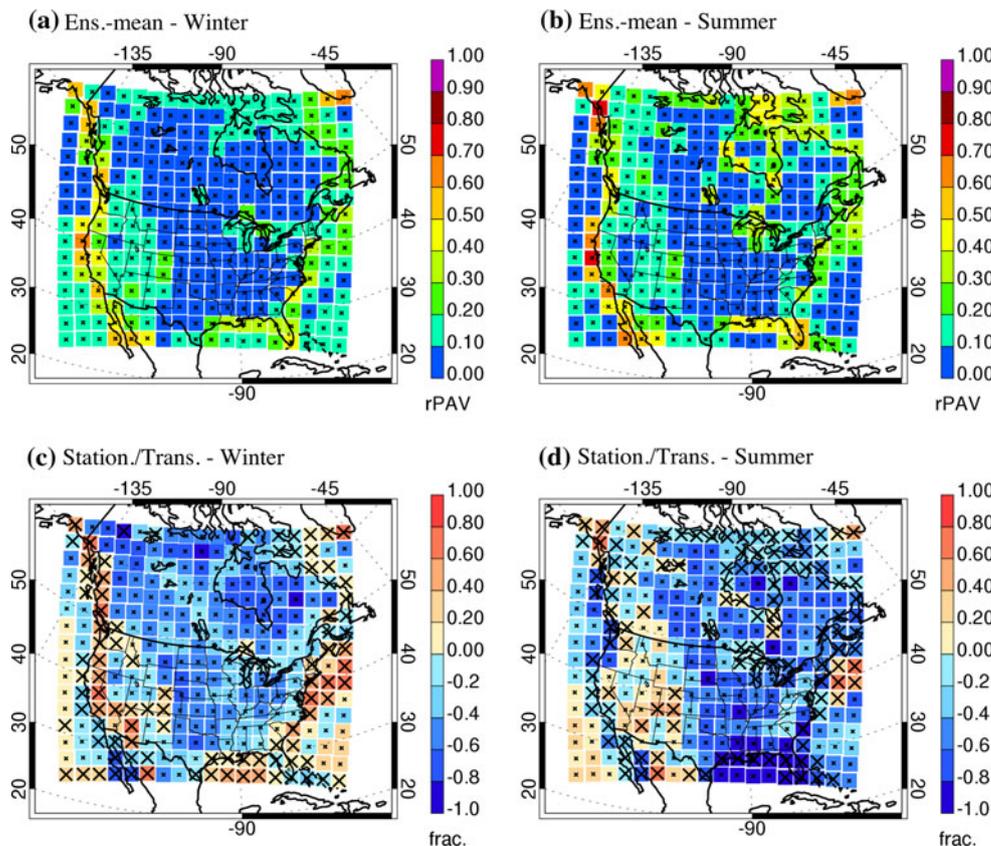
total variances in this season and the land-sea contrast intensification.

Cold season results show that regions with *rPAV* ≥ 15 % are dominated by the stationary term with only some exceptions in the West Coast and the Labrador Sea where the transient variance term tends to be more important. It is evident from Fig. 10c that *rPAV* values in the Atlantic Ocean regions are induced by the permanent and relatively strong temperature gradients across the Gulf Stream and not as a result of a transient mechanism. Similar results are found in warm season with only a marked dominance of the transient term in the Gulf of Mexico.

rPAV values derived from individual RCM simulations generally show similar results to the ensemble-mean *rPAV* although differences can appear over the Canadian Archipelago, the Great Lakes and other lakes in Canada. A more detailed analysis of the uncertainties arising in the computation of *rPAV* terms is presented in Appendix B.

4.3 Simple and more complex *rPAV* in mountainous regions

As discussed in the previous section, the PAV of high-resolution fields is mostly confined to those regions with significant influence of surface forcings. A fair question to ask is whether this PAV arises as a result of the influence of

complex surface mechanisms (e.g., land-sea breezes or terrain-enhanced triggering of hydrodynamics instabilities) or results from simple, maybe linear, interactions between the fine-scale forcing and the variable of interest.

One such a simple mechanism that seems to be important to explain *rPAV* in mountainous regions is related with the general relation between temperature and terrain elevation. The more detailed representation of terrain elevation gradients will create stationary temperature gradients even when no fine-scale atmospheric processes occur.

In order to test the influence of this last effect, the *rPAV* measure has been computed from a synthetic high-resolution 2-m temperature field derived using a linear relationship between the low-resolution VGCM temperature field and the high-resolution 50-km surface elevation field in the following way:

$$T_{RCM}^{orog} = T_{VGCM} + \Gamma \cdot h_{RCM}, \tag{6}$$

with T_{VGCM} the virtual GCM time series (in K), h_{RCM} the high-resolution topography (in km) of the RCM and $\Gamma = -6.5$ K/km the middle-latitude standard atmosphere (SA) lapse rate (see Dutton 1976 for a brief description). Equation (6) constitutes a crude way of taking into account the effects of changes in terrain-elevations when interpolating the temperature field into a higher resolution grid mesh. Several and important differences would appear

between the actual 2-m temperature topographic lapse rate and the free air SA lapse-rate approximation, starting from the fact that the effects of the surface in the adjacent temperature (e.g., sensible and latent heat fluxes) are not taken into account in the SA lapse rate. As shown by Prömmel et al. (2010), the use of the constant SA lapse rate along the year may lead to biases not caused by the models themselves, particularly in winter months where the atmosphere can be much more stable with mean lapse rates of the order of $\Gamma = -3.0\,K/km$.

In order to assess the similarity between the real stationary rPAV field and the artificial one, spatial correlations are computed using:

$$r = \frac{cov(rPAV_{stationary}, rPAV_{orog})}{\sigma(rPAV_{stationary})\sigma(rPAV_{orog})}, \qquad (7)$$

with $rPAV_{stationary}$ the original stationary RCM $rPAV$ and $rPAV_{orog}$ the $rPAV$ derived using Eq. (6) as input temperature. The linear correlation is computed only for those regions with relatively complex topography but with no influence of the land-water contrast forcing. Complex terrain regions are defined by a standard deviation of the elevation field within the region larger than 250 m. For each RCM, the land-sea mask is defined by the fraction of land inside each grid box with values varying between 0 and 1. Regions with important influence of land-water contrast are then defined as those with a water fraction standard deviation larger than 0.2. The total number of regions considered in correlation calculations depends on the RCM due to the different representation of both surface fields and grid location and varies between 37 (ECP2 model) and 51 (CRCM model) across models.

Table 2 shows the 90 % confidence interval of the linear correlations between $rPAV_{orog}$ and the stationary part of the rPAV term. Correlation confidence intervals are estimated using a Monte Carlo approach by sampling 1,000 times

Table 2 90 % confidence interval of the linear correlation coefficient between the stationary part of the $rPAV$ measure computed using RCM simulations and the $rPAV$ derived using the low-resolution VGCM temperature field and the high-resolution topographic field (see Sect. 4.3 for a detailed explanation)

	Cold season	Warm season
CRCM	[0.82; 0.96]	[0.72; 0.94]
MM5I	[0.87; 0.97]	[0.72; 0.94]
ECP2	[0.81; 0.93]	[0.35; 0.78]
RCM3	[0.88; 0.97]	[0.68; 0.92]
WRFG	[0.83; 0.96]	[0.71; 0.92]
HRM3	[0.81; 0.96]	[0.81; 0.92]
RCMs-MEAN	[0.84; 0.96]	[0.67; 0.90]

Only those regions characterized by complex topography (see the text for its definition) with no land-sea contrasts are included in the calculation

randomly with replacement over both spatial series. The 90 % confidence interval is then computed by calculating the 5th and the 95th percentiles of the 1,000-elements correlation distribution.

In both seasons and for every single RCM, correlations between the $rPAV_{orog}$ and the stationary $rPAV$ are very high with an RCM-mean 5th (95th) percentile value of 0.84 (0.96) and 0.67 (0.90) in cold and warm seasons respectively. This suggests that about 80 and 65 % of the RCM $rPAV$ variance is linearly explained by the orographically-induced field in cold and warm seasons, respectively.

Inter-model differences are generally small, of the order of 10 % of the mean correlations, and contained within the sampling errors as estimated from the 5th and 95th percentile differences, which are generally of the order of 15–20 %, but can be as high as 40 %.

5 PAV in the climate change signal (AOGCM driven simulations): preliminary results

So far, we have analyzed the potential of RCMs to add value over their associated virtual-GCMs in the simulation of temperature in present-climate conditions (i.e., driven by NCEP reanalyses). This information can be useful in a broad spectrum of RCM applications such as the reconstruction of recent-past climate on the regional scale (e.g., Mesinger et al. 2006; Kanamitsu and Kanamaru 2007), the downscaling of low-resolution global simulations in seasonal-prediction investigations (e.g., Rauscher et al. 2007; Seth et al. 2007; De Sales and Xue 2011) and the study of processes and mechanisms in the regional scale (Pielke et al. 1999; Roebber and Gyakum 2003).

One of the main applications of RCMs in the last decade has been its use to downscale future-climate projections produced by coupled GCMs. In order to account for systematic biases in RCM projections, a popular approach used to estimate high-resolution future climate is through the "delta method" (e.g., see Rummukainen 2010). The delta method consists of modifying the observed high-resolution climate data with the RCM climate change (CC) signal to obtain an unbiased version of the future projection. This suggests that the RCM's added value in climate projections may not come directly from the simulation of future scenario periods but from the climate-change signal itself. While the problem of looking for PAV in the CC signal is intimately related with that of PAV in present climate, some differences appear.

The CC signal of the time-averaged temperature field is defined in the usual way by computing the difference between the time-mean field in present and future conditions. Using the same notation as in Sect. 3 we have:

$$CC_{RCM_i} \equiv CC_i = \overline{T}_i(future) - \overline{T}_i(present), \qquad (8)$$

with CC_{RCM_i} the high-resolution CC signal over the ith 300-km side region. Following the ideas used for the present-climate PAV framework, we can aggregate CC_{RCM_i} over 300-km side regions in order to produce a low-resolution version of the CC signal that we denote by CC_{VGCM}.

A question that arises naturally in the context of the PAV framework is whether the high-resolution CC field contains fine-scale information that is absent in the low-resolution part. Given that some of the most important sources of climate change are large scale in nature (e.g., CO_2 concentration changes, water vapor feedback, etc), it is unclear whether the CC signal should contain a large high-resolution component. A simple way to quantify the relative importance of fine and large scales in the high-resolution CC signal can be done by defining:

$$rPAV^{CC} = \frac{\sigma(CC_{RCM_i})}{mean(CC_{RCM_i})} = \frac{\sigma(CC_{RCM_i})}{CC_{VGCM}}, \qquad (9)$$

where $\sigma(CC_{RCM_i})$ denotes the spatial standard deviation of the high-resolution CC signal field (CC_{RCM_i}) and CC_{VGCM} the mean temperature change between future and present periods over the region of interest. With this definition $rPAV^{CC} \sim 0$ would suggest that the high-resolution estimation does not add extra information over the coarse-resolution one and, $rPAV^{CC} \sim 1$ would suggest that the

fine-scale contributions can be as large as the large-scale mean temperature change.

Again, it should be emphasised that the PAV measure as defined in Eq. (9) only accounts for the PAV small scales (PAV^{ss}), that is, the PAV arising from the simulation of fine-scale features that are absent in GCM fields. The ratio $rPAV^{CC}$ is mute about the potential of RCMs to add value in large scale variables (i.e., PAV^{ls}).

Figure 11a and b show the CC_{RCM_i} field for the CRCM-CGCM3 simulation in cold and warm seasons respectively. In both seasons, results show warmer conditions in the future with a stronger signal in continental compared to oceanic regions. In cold season, the spatial pattern of CC_{RCM_i} shows a general increase to the north and to the interior of the continent that attains almost 7 K in the centre of the Hudson Bay (2041–2065 minus 1971–1995). In warm season the spatial pattern of CC_{RCM_i} shows maximum values in continental-middle latitudes with changes as large as 4 K in central United States. Other RCM-AOGCM couples show similar spatial patterns of mean-temperature changes in cold season (not shown).

Figure 11c and d show the $rPAV^{CC}$ measure for the CRCM-CGCM3 simulation in cold and warm seasons, respectively. In both seasons, $rPAV^{CC}$ values are generally smaller than 10 % with values somewhat higher in warm compared to cold season, particularly in coastline regions.

Fig. 11 High-resolution climate change signal (*top panels*) and the $rPAV^{CC}$ measure (*bottom panels*) in cold (*left panels*) and warm (*right panels*) seasons. Results correspond to the CRCM-CGCM3 simulation. Only values smaller than 0.6 are shown in **c** and **d**
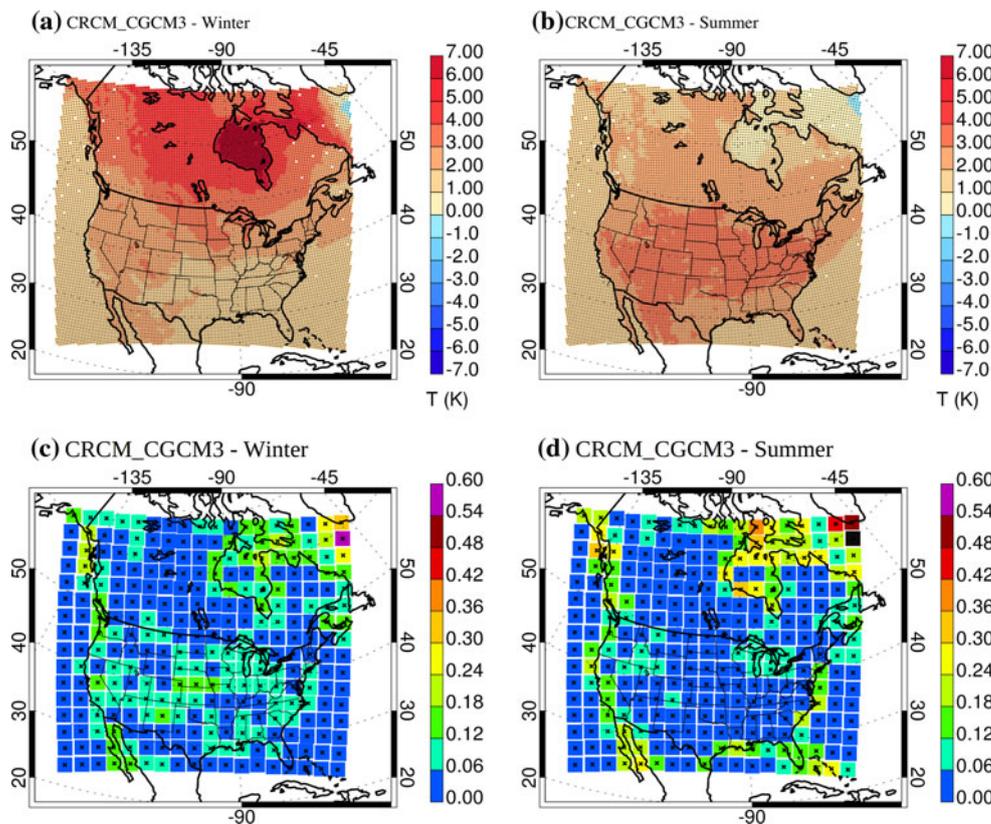
The largest values in coastline regions result from the differential warming observed in land and water surfaces.

Figures 12 and 13 show the $rPAV^{CC}$ measure for the other individual RCM-AOGCM simulations (Figs. 12a–e and 13a–e) and for the ensemble-mean (Figs. 12f and 13f) results in cold and warm seasons respectively. Most models show similar results to the CRCM-CGCM3 simulation, with relatively small $rPAV^{CC}$ values everywhere, maxima in coastline regions and somewhat larger values in warm compared to cold season results. The WRFG-CCSM simulation shows very large $rPAV^{CC}$ values over lake regions in warm season (see Fig. 13) but this seems to be related with a different representation of lakes in present and future conditions.

Maybe the most interesting feature is related with the robustness of the $rPAV^{CC}$ results. Black squares in Figs. 12f and 13f denote regions in which $rPAV^{CC}$ satisfies two conditions: that the RCM ensemble-mean $rPAV^{CC}$ is larger than twice the inter-model standard deviation, and larger than 5 %. That is, black squares identify those regions in which a significant $rPAV^{CC}$ signal is robust across the different RCM simulations.

In cold season, robust regions (59 out of 288) appear along the North American West Coast, in most coastline regions in the Hudson Bay and in some regions with important fine scale topography in the Rocky Mountains. In warm season, robust regions (60 out of 288) appear along the East and West Coasts with coastline regions over the Hudson Bay appearing as non-robusts.

6 Discussion

The use of RCMs to dynamically downscale large-scale atmospheric fields in present and future climate conditions has gained popularity as a way to circumvent the spatial scale gap that exists between the climate information provided by AOGCMs and the input needed in impact and adaptation studies. There is still a need, however, to objectively quantify the gains arising from the use of RCMs as climate downscaling tools.

In this article we use the "potential added value" framework proposed in Di Luca et al. (2012) with the aim of detecting the regions and seasons where RCMs show potential to improve the simulation of temperature statistics compared to the driving models. This detection is performed by looking for regions and seasons showing a large contribution of fine-scale details on the climate statistics of interest. The presence of fine-scale variance is interpreted as a necessary condition for a RCM simulation to add value. It should be clear, however, that the actual added value will depend on how the simulated climate compares with the observed one and will always be smaller or equal than the PAV.

The methodological approach used in this paper can be summarised through three main steps:

1. 20-year 3-hourly time series of near-surface temperature fields simulated by 6 RCMs are decomposed using
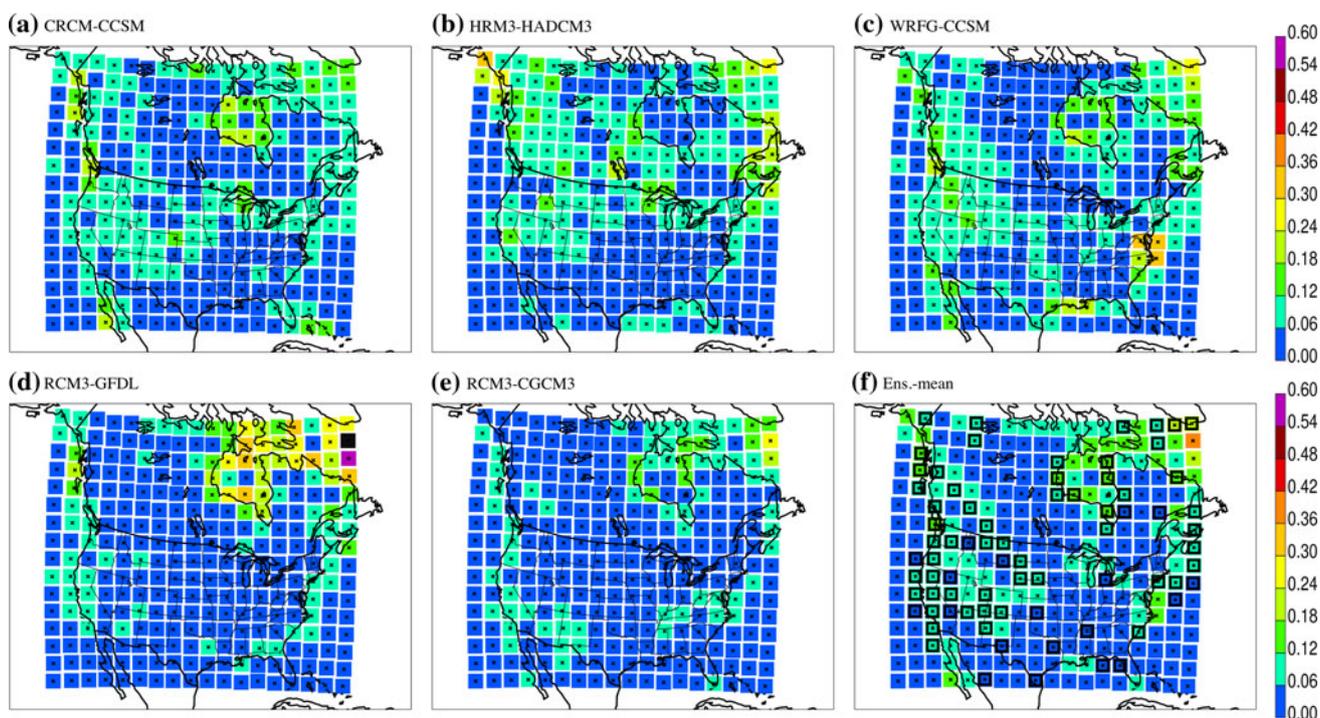
Fig. 12 The $rPAV^{CC}$ measure in cold season as computed from individual RCM simulations (**a–e**) and from the ensemble-mean field (**f**)
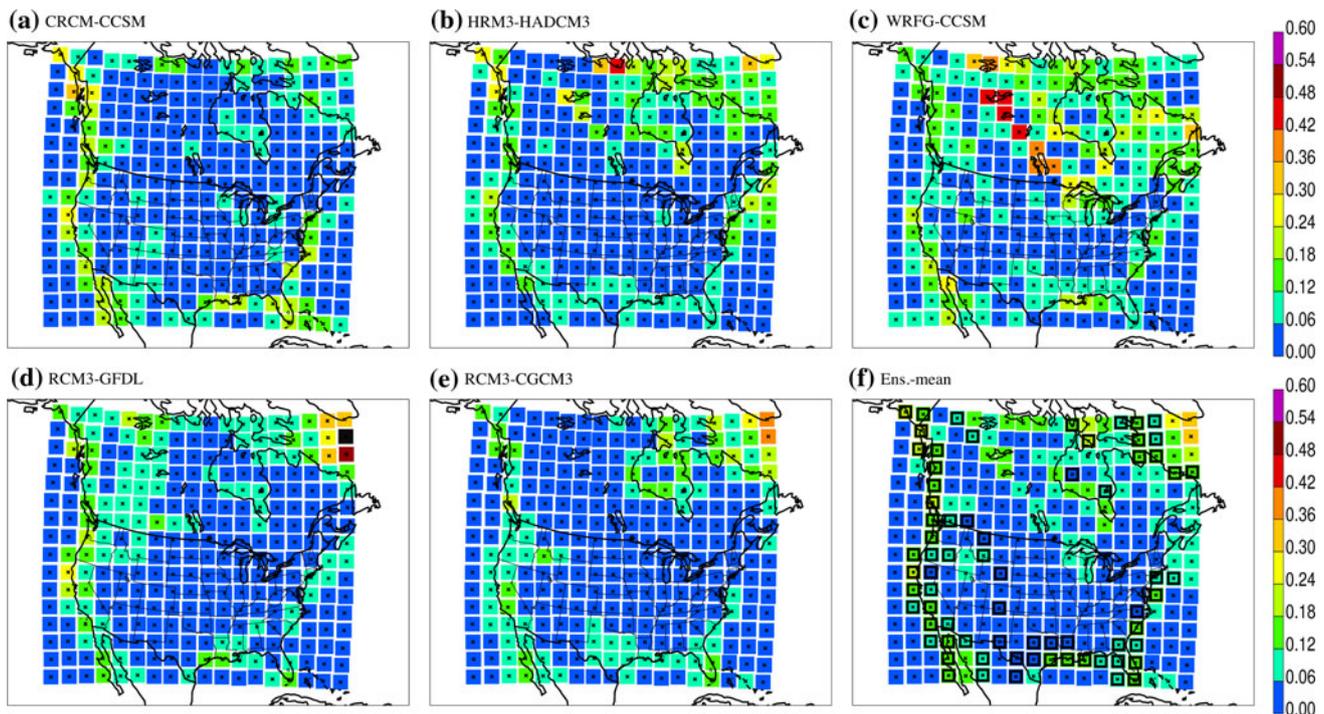
Fig. 13 As in Fig. 12 but for warm season computations

Reynolds averaging rules. The temperature field over 300 km by 300 km regions (i.e., approximately equivalent to GCM grid boxes and containing several RCM grid points) is separated in four terms: the spatio-temporal mean, a time series describing the temporal fluctuations of the spatial mean, a time-averaged field of the spatial-mean deviations and a residual time varying field containing the spatio-temporal fluctuations.

2. In each 300-km side regions, the variance of the high-resolution temperature field is then described by three terms that result from the Reynolds decomposition. The first is the temporal variance of the spatial-mean field that is assumed to represent the GCM contribution to the total variance. The other two terms depend on the spatial deviations and are related with the stationary (time mean) and transient RCM contributions to the total variance.

3. The PAV is then defined as sum of the fine-scale stationary and transient RCM variances. A normalised quantity (*rPAV*) is defined by computing the fraction of the total variance that is explained by RCM variances.

Our results indicate that, independently of the season considered, the high-resolution near-surface temperature variance is mostly explained by the virtual-GCM term, with a contribution from the RCM terms that is generally smaller than 15 % but can attain 60–70 % in some regions.

The contribution from the fine-scale stationary and transient terms is roughly of the same order of magnitude but they are induced by different mechanisms and therefore they show distinct spatial patterns of variability.

The fine-scale stationary spatial variance term is sensitive to time-averaged temperature gradients and is hence important in regions where surface forcings are important either due to complex topography or land-sea contrast (i.e., with coastlines or lakes). The stationary term can also arise due to the presence of strong stationary gradients from other sources such as the strong SSTs variation over the Gulf Stream.

The fine-scale transient variance term is associated with spatial differences in the temporal variability of 2-m temperature and seems to be dominated by two mechanisms. A first mechanism is related with the presence of land-sea contrast and describes the differential temporal variability of temperature in land and water grid points. A clear example of this mechanism is given by the different diurnal cycle over land and water grid points. The second mechanism is independent of the fine-scale surface forcings and describes the spatial variability induced by the passage of weather disturbances, mainly of synoptic scale. This last term appears to be more important in winter and over high-latitudes due to the stronger intensity and variability of synoptic-scale systems. In addition, due to the dominant thermal-inertia effect of ocean waters on 2-m temperature, this term is also stronger over the continent.

When computing the fraction of the total variance explained by RCM terms, we find that relatively large values of *rPAV* are essentially confined to regions with important surface forcings mainly due to land-sea contrasts. In general, but particularly in coastline high-latitude regions, *rPAV* tends to be larger in warm than in cold season due to an intensification of the land-sea contrast forcing related with ice/snow cover in cold season and a much stronger diurnal cycle in warm season.

In Sect. 5, the potential of RCMs to add value over lower resolution models in reproducing the climate-change (CC) signal is discussed. It is stressed that the existence of PAV in present climate does not imply that PAV will be present in the CC signal. Our results show that the fine-scale spatial variability in the high-resolution CC temperature over the 300-km side regions is generally one order of magnitude smaller than the mean CC signal itself. The analysis indicates that the largest potential AV appears in coastline regions due to the differential warming in land and water surfaces. This effect tends to be more pronounced in warm than in cold season. It is seen that, in mountainous regions, the PAV present in present climate is almost lost in the CC signal; this results mainly from the fact that, as shown in Sect. 4, the PAV in mountainous regions is dominated by quasi-linear stationary processes that are very similar in present and future climate and hence tend to be cancelled out when computing the CC signal.

In general, results point out that the potential of RCMs to add value in near-surface temperature is rather limited in oceanic and flat regions with little land-sea contrast and fine-scale topography. This result agrees with previous studies of Winterfeldt and Weisse (2009) and Winterfeldt et al. (2011) who showed similar results for the study of marine near-surface winds over oceanic and coastal regions. Also, our results are in agreement with those from Prömmel et al. (2010) who found that over the Greater Alpine Region their RCM adds value over the ERA40 reanalysis only in the more complex topography subregions. Furthermore, even for those regions showing relatively large *rPAV* values, it remains to be seen whether this added value could not be obtained using simple, maybe even linear, relationships between the high-resolution surface forcing and the low-resolution variable of interest. An example of such a simple relation was shown in Sect. 4.3.

Feser (2006) indicated that the AV can be strongly dependent on the variable used in the analysis by showing much higher AV in the 2-m temperature field compared to the sea level pressure field. Similarly, we applied the variance decomposition methodology to the time-varying precipitation and results (not shown) suggest that the relative influence of RCM contributions to the total variance

is larger in precipitation than in 2-m temperature. For example, for 3-hourly time varying fields, the ensemble-mean domain average rPAV in cold (warm) season is 5 % (16 %) for temperature and 23 % (40 %) for precipitation. These results together with those from Di Luca et al. (2012) suggest that efforts aiming to show the benefits of using RCMs over lower resolution GCMs should concentrate on moist processes or in climate statistics with significant fine-scale variability such as high-order statistics variables with large spectral power at high temporal frequencies.

Finally, two important caveats should be discussed regarding our results. First, as discussed in the methodology Section, this work and the previous study by Di Luca et al. (2012), concentrated on the potential added value on the small spatial scales, disregarding the possible impact of high-resolution simulations on larger scales. It was assumed that spatial average of RCM quantities within an area equivalent to the driving model grid-box is identical to the driving model grid-box value. This necessarily precludes any analysis of possible improvements at that scale. The second caveat relates to the fact that our methodology may be badly suited to detect potential added value of complex characteristics. For example, phenomena such as downslope winds near mountain ranges or lake-effect snowfall may need a methodology tailored to that particular objective.

Appendix A: Variance decomposition

The high-resolution temperature field as simulated by any RCM can be decomposed in its spatial-mean and spatial-fluctuations as:

$$T_{i,k} = \overline{T_{i,k}}^i + \widehat{T}_{i,k}$$
$$= VGCM_k + RCM_{i,k}, \tag{10}$$

where $\overline{(.)}$ denotes the arithmetic average over grid points (i) or time (k). $VGCM_k$ is the virtual GCM term given by the time series of the spatial mean and $RCM_{i,k}$ the RCM term representing the time series of the spatial deviations:

$$RCM_{i,k} = T_{i,k} - \overline{T_{i,k}}^i. \tag{11}$$

Similarly, each time varying term in Eq. (10) can be decomposed into a stationary and a transient part as:

$$VGCM_k = \overline{T_{i,k}}^i = \overline{\left(\overline{T_{i,k}}^i\right)}^k + \left(\overline{T_{i,k}}^i\right)'$$
$$= sVGCM + tVGCM_k, \tag{12}$$

and

$$RCM_{i,k} = T_{i,k} - \overline{T_{i,k}}^i = \overline{\left(\widehat{T}_{i,k}\right)}^k + \left(\widehat{T}_{i,k}\right)'$$
$$= sRCM_i + tRCM_{i,k}, \tag{13}$$

where

$$tVGCM_k = \overline{T_{i,k}}^i - \overline{\left(\overline{T_{i,k}}^i\right)}^k$$
$$= VGCM_k - \overline{VGCM_k}^k \tag{14}$$

and

$$tRCM_{i,k} = T_{i,k} - \overline{T_{i,k}}^i - \overline{\widehat{T}_{i,k}}^k$$
$$= RCM_{i,k} - \overline{RCM_{i,k}}^k. \tag{15}$$

From Eqs. (10), (12) and (13) we obtain,

$$T_{i,k} = sVGCM + tVGCM_k + sRCM_i + tRCM_{i,k}. \tag{16}$$

The sample variance of Eq. (16) is given by,

$$\sigma^2 = \overline{\overline{(T_{i,k} - sVGCM)^2}^k}^i$$
$$= \overline{\overline{(tVGCM_k + sRCM_i + tRCM_{i,k})^2}^k}^i$$
$$= \overline{\overline{(tVGCM_k)^2}^k}^i + \overline{\overline{(sRCM_i)^2}^k}^i + \overline{\overline{(tRCM_{i,k})^2}^k}^i$$
$$+ 2(\overline{tVGCM_k}^k \overline{sRCM_i}^i)$$
$$+ 2\overline{(tVGCM_k \overline{tRCM_{i,k}}^i)}^k \tag{17}$$

From Eqs. (14) and (15) it follows that $\overline{tVGCM_k}^k = 0$ and $\overline{tRCM_{i,k}}^k = 0$. Hence, without any approximation, Eq. (16) can be writen as:

$$\sigma^2 = \sigma^2_{tVGCM_k} + \sigma^2_{sRCM_i} + \sigma^2_{tRCM_{i,k}} + 2\overline{(tVGCM_k \overline{tRCM_{i,k}}^i)}^k. \tag{18}$$

The PAV term can then be defined by the sum of those terms that include any contribution from the RCM. In practice, the covariance term $2\overline{(tVGCM_k \overline{tRCM_{i,k}}^i)}^k$ is at least 10 times smaller (not shown) than the sum of other two contributions so it is neglected in the analysis.

The variance decomposition can be applied independently to each RCM dataset. That is, for each model m we obtain:

$$\sigma^2|_m = \sigma^2_{tVGCM_k}|_m + \sigma^2_{sRCM_i}|_m + \sigma^2_{tRCM_{i,k}}|_m. \tag{19}$$

The ensemble-mean for each variance term is then obtained by computing the arithmetic mean over all models. For the total variance the expression is given by:

$$\overline{\sigma^2|_m}^m = \frac{1}{M}\sum_m \sigma^2|_m, \tag{20}$$

and similar expressions for the other variance terms.

Appendix B: Uncertainties in rPAV estimations

In order to examine how robust are the PAV results, we consider some of the uncertainties arising in the estimation of variances from the RCM simulated temperature time series. Two types of uncertainties are partially (roughly) assessed: uncertainty due to the natural variability of the climate system and the RCM structural uncertainty due to our incomplete knowledge of the climate system and the resulting differences in the representation of some processes in the several RCMs.

Inherent to the process of computing a climate statistics from a finite lengh time series (i.e., 20 years periods in our case) there is an uncertainty related with sampling variability. In order to get a quantitative measure of this uncertainty, variances in Eq. (3) have been estimated using a Monte Carlo approach. That is, each variance term is computed 500 times by sampling randomly with replacement over the original time varying field $T_{i,k}$. Traditional bootstrapping methods (Efron and Tibshirani 1993) rest on the assumption that the data of analysis are composed of independent samples, an hypothesis that is evidently not true in the case of the 3-hourly and 50-km temperature fields used to estimate variance terms. In order to account for the serial (or auto-) correlation in the temporal dimension, the temporal sampling is performed by randomly selecting a subset of the total data assuming that temperature values are independent every three days. This is equivalent to use a variance inflation factor as described in Wilks (2010). In the spatial dimension, the bootstrapping is performed assuming that adjacent grid points are independent, an hypothesis that we know is not adequate.

For each RCM, an estimation of the uncertainty can then be obtained by computing, for example, the standard deviation of the distribution of each variance term containing the 500 samples. The PAV sampling uncertainty can then be defined as the sum of the stationary and transient sampling standard deviations. In a similar way, the rPAV sampling uncertainty for each RCM can be obtained by computing the standard deviation of the rPAV Monte Carlo distribution. Figure 14a and b show the ratio between the inter-model mean rPAV sampling standard deviation and RCM ensemble-mean rPAV for cold and warm seasons respectively. In both seasons, the sampling uncertainty pattern resembles the ensemble-mean rPAV pattern showing relatively uniform fields for the ratio between both. Inter-model mean values, but also individual model results (not shown), show domain-mean values of about

~15 % in both seasons, with values that can attain up to 50 % in some regions. As clear from Fig. 14a and b, the largest values of the sampling ratio arise in those regions that have the borders near the coast (i.e., with maybe only one grid point that differs from all the others).

A simple measure of the RCMs' uncertainty can be obtained by quantifying the spread between RCMs through the multi-model standard deviation. The unbiased formula of the standard deviation (von Storch and Zwiers 1999) is desirable because of the small number of simulations available for the analysis (in what follows, we use always the unbiased formula when computing the inter-model spread). Figure 14c and d show the ratio between the inter-model standard deviation and RCM ensemble-mean rPAV for cold and warm seasons respectively. Values of the ratio are larger than in the sampling uncertainty case particularly

Fig. 14 Inter-model mean sampling uncertainty in (**a**) cold and (**b**) warm seasons. RCMs uncertainty in (**c**) cold and (**d**) warm seasons. **e** shows the inter-model standard-deviation of the standard deviation of the surface-fraction field
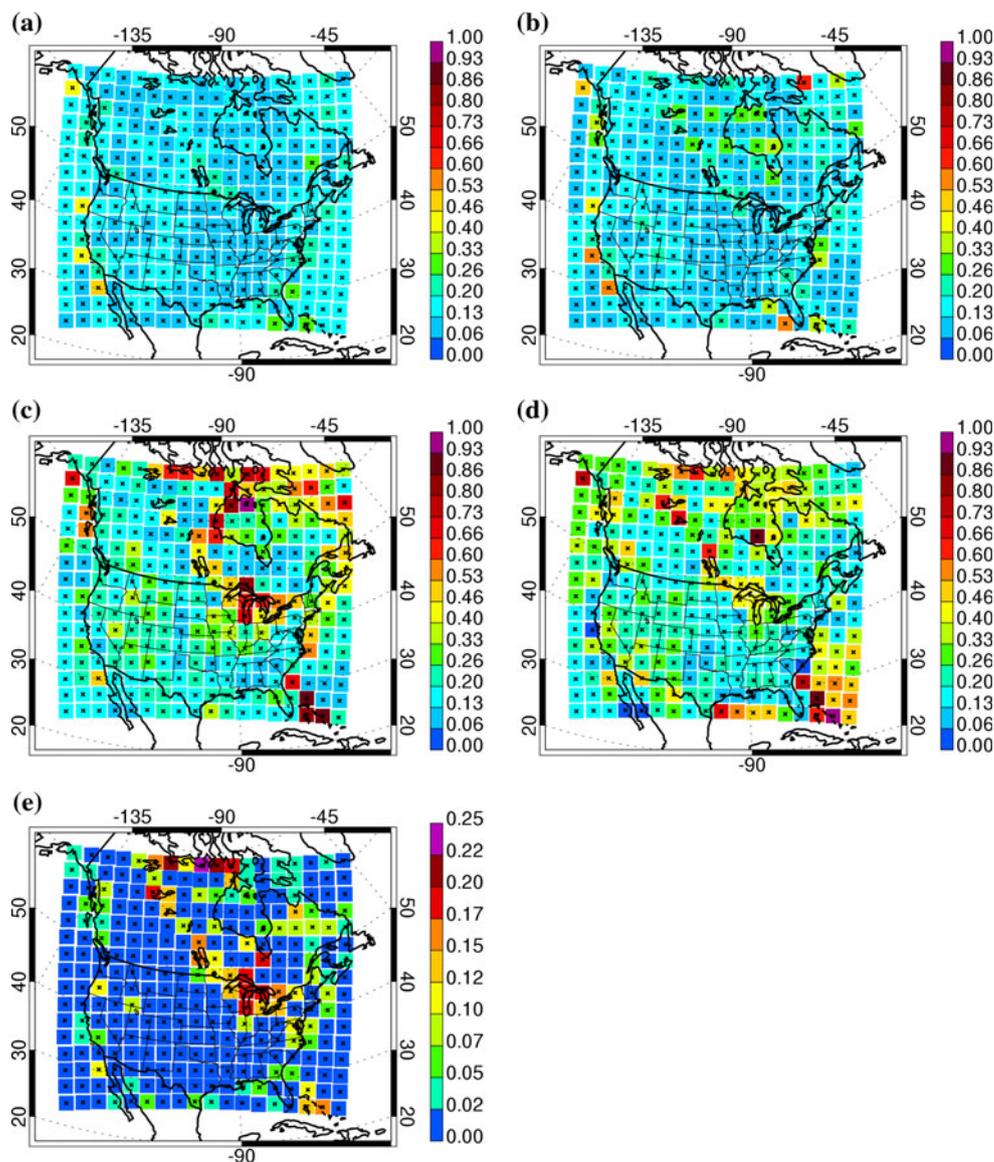
in some oceanic and coastline regions. In general, however, the standard deviation represents less than 20–30 % of the signal showing that there is a relative large agreement between RCM simulations.

Assuming that robust features across RCMs are those for which the signal (i.e., the RCM ensemble-mean) is at least two times larger than the RCM spread, some regions can be pointed out to be non robust (not shown). In cold season, non-robust regions appear in the Atlantic Ocean in the southern part of the domain, in some high-latitude regions and near the Great Lakes. Models' uncertainties in some of these regions appear to be related with differences in the land-water fraction masks used by each RCM. For example, the RCM3 model does not contain any lake and WRFG contains only the largest lakes. Figure 14e shows the multi-model standard deviation of the land-fraction standard deviation in each 300-km side region. The largest differences across RCMs arise near the Canadian Archipelago, the Great Lakes and others lakes in Canada, and in the Atlantic Ocean near Florida due to the presence of some islands.

Open Access   This article is distributed under the terms of the Creative Commons Attribution License which permits any use, distribution, and reproduction in any medium, provided the original author(s) and the source are credited.

References

Castro CL, Pielke RA, Leoncini G (2005) Dynamical downscaling: an assessment of value added using a regional climate model. J Geophys Res 110:D05,108. doi:10.1029/2004JD004721

Caya D, Laprise R (1999) A semi-implicit semi-lagrangian regional climate model: the Canadian RCM. Mon Wea Rev 127(3): 341–362

Collins WD, Bitz CM, Blackmon ML, Bonan GB, Bretherton CS, Carton JA, Chang P, Doney SC, Hack JJ, Henderson TB, Kiehl JT, Large WG, McKenna DS, Santer BD, Smith RD (2006) The community climate system model version 3 (ccsm3). J Clim 19:2122–2143. doi:10.1175/JCLI3761.1

De Sales F, Xue Y (2011) Assessing the dynamic downscaling ability over South America using the intensity-scale verification technique. Int J Climatol 31:1205–1221. doi:10.1002/joc.2139

Di Luca A, de Elía R, Laprise R (2012) Potential for added value in precipitation simulated by high-resolution nested regional climate models and observations. Clim Dyn 38:1229–1247. doi:10.1007/s00382-011-1068-3

Dickinson R, Errico R, Giorgi F, Bates G (1989) A regional climate model for the western United States. Clim Change 15:383–422

Dutton J (1976) The ceaseless wind. McGraw-Hill, New York, NY

Efron B, Tibshirani R (1993) An introduction to the bootstrap, monographs on statistics and applied probability. vol 57, Chapman and Hall, London

Feser F (2006) Enhanced detectability of added value in limited-area model results separated into different spatial scales. Mon Wea Rev 134:2180–2190

Feser F, Rockel B, von Storch H, Winterfeldt J, Zahn M (2011) Regional climate models add value to global model data: a review and selected examples. Bull Am Meteorol Soc doi: 10.1175/2011BAMS3061.1

Flato G (2005) The third generation coupled global climate model (CGCM3). Available from http://wwwecgcca/ccmac-cccma/

GFDL Global Atmospheric Model Development Team (2004) The new GFDL global atmosphere and land model am2–lm2: evaluation with prescribed sst simulations. J Clim 17(24):4641–4673, doi: 10.1175/JCLI-3223.1, http://journals.ametsoc.org/doi/abs/10.1175/JCLI-3223.1, http://journals.ametsoc.org/doi/pdf/10.1175/JCLI-3223.1

Giorgi F, Bates G (1989) The climatological skill of a regional model over complex terrain. Mon Wea Rev 117:2325–2347

Giorgi F, Mearns L (1991) Approaches to the simulation of regional climate change: a review. Rev Geophys 29:191–216

Giorgi F, Marinucci M, Bates G (1993) Development of a second generation regional climate model (regcm2) i: boundary layer and radiative transfer processes. Mon Wea Rev 121:2794–2813

Giorgi F, Christensen J, Hulme M, von Storch H, Whetton P, Jones R, Mearns L, Fu C, Arritt R, Bates B, Benestad R, Boer G, Buishand A, Castro M, Chen D, Cramer W, Crane R, Crossly J, Dehn M, Dethloff K, Dippner J, Emori S, Francisco R, Fyfe J, Gerstengarbe F, Gutowski W, Gyalistras D, Hanssen-Bauer I, Hantel M, Hassell D, Heimann D, Jack C, Jacobeit J, Kato H, Katz R, Kauker F, Knutson T, Lal M, Landsea C, Laprise R, Leung L, Lynch A, May W, McGregor J, Miller N, Murphy J, Ribalaygua J, Rinke A, Rummukainen M, Semazzi F, Walsh K, Werner P, Widmann M, Wilby R, Wild M, Xue Y (2001) Regional climate information- evaluation and projections. In: Houghton JT (eds) Climate change 2001: the scientific basis. Contribution of working group I to the third assessment report of the intergovernmental panel on climate change, Cambridge University Press, Cambridge, pp 583–638

Giorgi F, Jones C, Asrar G (2009) Addressing climate information needs at the regional level: the CORDEX framework. WMO Bull 58:175–183

Gordon C, Cooper C, Senior C, Banks H, Gregory J, Johns T, Mitchell J, Wood R (2000) The simulation of sst, sea ice extents and ocean heat transports in a version of the Hadley Centre coupled model without flux adjustments. Clim Dyn 16:147–168. doi:10.1007/s003820050010

Grell JD G, Stauffer DR (1993) A description of the fifth-generation Penn State/NCAR mesoscale model (MM5). National Center for Atmospheric Research, ncar/tn-398 1 ia edn

Jones RG, Noguer M, Hassel DC, Hudson D, Wilson SS, Jenkins GJ, Mitchell JFB (2004) Generating high resolution climate change scenarios using precis. Tech. rep., Met Office Hadley Centre

Juang HMH, Hong SY, Kanamitsu M (1997) The NCEP regional spectral model: an update. Bull Am Meteorol Soc 78:2125–2143

Kanamitsu M, Kanamaru H (2007) Fifty-seven-year California reanalysis downscaling at 10 km (CaRD10). Part i: system detail and validation with observations. J Clim 20(22):5553–5571

Kanamitsu M, Ebisuzaki W, Woollen J, Yang SK, Hnilo J, Fiorino M, Potter G (2002) NCEP-DOE AMIP-II reanalysis (R-2). Bull Am Meteorol Soc 83(11):1631–1643

Laprise R, Jones R, Kirtman B, von Storch H, Wergen W (2002) Atmospheric regional climate models (RCMs): a multiple purpose tool? Tech. rep., Report of the joint WGNE/WGCM ad hoc panel on regional climate modelling

Laprise R, de Elía R, Caya D, Biner S, Lucas-Picher P, Diaconescu E, Leduc M, Alexandru A, Separovic L (2008) Challenging some tenets of regional climate modelling. Meteor Atmos Phys 100, Special Issue on Regional Climate Studies (20):3–22

Leung L, Done J, Dudhia J, Henderson T, Vertenstein M, Kuo B (2005) Preliminary results of WRF for regional climate simulations. In: Workshop research needs and directions of regional

climate modeling using WRF and CCSM, Boulder, CO, 6, pp 833–854. Available from http://www.cs.berkeley.edu/~luca/cs278/notes/lecture09.pdf

Mearns L, Gutowski W, Jones R, Leung R, McGinnis S, Nunes A, Qian Y (2009) A regional climate change assessment program for North America. Eos Trans AGU 90(36):311

Mesinger F, Brill K, Chuang HY, DiMego G, Rogers E (2002) Limited area predictability: can "upscaling" also take place? Tech. Rep. 32, 5.30–5.31, Research activities in atmospheric and oceanic modelling, WMO, CAS/JSC WGNE, Geneva

Mesinger F, DiMego G, Kalnay E, Mitchell K, Shafran P, Ebisuzaki W, Jovic D, Woollen J, Rogers E, Berbery E, Ek M, Fan Y, Grumbine R, Higgins W, Li H, Lin Y, Manikin G, Parrish D, Shi W (2006) North american regional reanalysis. Bull Am Meteorol Soc 87:343–360

Pielke R, Wlako R, Steyaert L, Vidale P, Liston G, Lyons W (1999) The influence of anthropogenic landscape changes on weather in south Florida. Mon Wea Rev 127:1663–1673

Prömmel K, Geyer B, Jones J, Widmann M (2010) Evaluation of the skill and added value of a reanalysis-driven regional simulation for alpine temperature. Int J Climatol 30:760–773

Randall D, Wood R, Bony S, Colman R, Fichefet T, Fyfe J, Kattsov V, Pitman A, Shukla J, Srinivasan J, Stouffer R, Sumi A, Taylor K (2007) Climate models and their evaluation. In: Solomon S, Qin D, Manning M, Chen Z, Marquis M, Averyt K, Tignor M, Miller H (eds) Climate change 2007: the physical science basis. contribution of working group I to the fourth assessment report of the intergovernmental panel on climate change, Cambridge University Press, Cambridge

Rauscher S, Seth A, Liebmann B, Qian JH, Camargo S (2007) Regional climate model-simulated timing and character of seasonal rains in South America. Mon Wea Rev 135:2642–2657

Roebber PJ, Gyakum JR (2003) Orographic influences on the mesoscale structure of the 1998 ice storm. Mon Wea Rev 131(1):27–50

Rummukainen M (2010) State-of-the-art with regional climate models. WIRE Adv Rev 1(1):82–96

Seth A, Rauscher S, Camargo S, Qian JH, Pal J (2007) Regcm regional climatologies for South America using reanalysis and ECHAM model global driving fields. Clim Dyn 28:461–480

Stull R (1988) An introduction to boundary layer meteorology. Kluwer Acad Publ, Morwell, USA

Veljovic K, Rajkovic B, Fennessy MJ, Altshuler EL, Mesinger F (2010) Regional climate modeling: Should one attempt improving on the large scales? Lateral boundary condition scheme: any impact. Meteorol Z 19(3):237–246

von Storch H, Zwiers F (1999) Statistical analysis in climate research. Cambridge Univesity Press, Cambridge

Wang Y, Leung L, McGregor J, Lee DK, Wang WC, Ding Y, Kimura F (2004) Regional climate modeling: progress, challenges, and prospects. J Meteor Soc Japan 82(6):1599–1628

Wilks D (2010) Sampling distributions of the Brier score and Brier skill score under serial dependence. Q J R Meteorol Soc 136:2109–2118

Winterfeldt J, Weisse R (2009) Assessment of value added for surface marine wind speed obtained from two regional climate models. Mon Wea Rev 137:2955–2965

Winterfeldt J, Geyer B, Weisse R (2011) Using quikscat in the added value assessment of dynamically downscaled wind speed. Int J Climatol 31:1028–1039. doi:10.1002/joc.2105